Reduced expression of phosphatase PTPN2 promotes pathogenic conversion of Tregs in autoimmunity

Mattias N.D. Svensson,[1,2] Karen M. Doody,[2] Benjamin J. Schmiedel,[3] Sourya Bhattacharyya,[3] Bharat Panwar,[3] Florian Wiede,[4] Shen Yang,[1] Eugenio Santelli,[1] Dennis J. Wu,[1,2] Cristiano Sacchetti,[1,2] Ravindra Gujar,[3] Gregory Seumois,[3] William B. Kiosses,[5] Isabelle Aubry,[6] Gisen Kim,[7] Piotr Mydel,[8,9] Shimon Sakaguchi,[10,11] Mitchell Kronenberg,[7] Tony Tiganis,[4,12,13] Michel L. Tremblay,[6] Ferhat Ay,[3] Pandurangan Vijayanand,[3] and Nunzio Bottini[1,2]

[1]Department of Medicine, University of California, San Diego, La Jolla, California, USA. [2]Division of Cellular Biology, and [3]Division of Vaccine Discovery, La Jolla Institute for Allergy and Immunology, La Jolla, California, USA. [4]Peter MacCallum Cancer Centre, Melbourne, Victoria, Australia. [5]Core Microscopy, La Jolla Institute for Allergy and Immunology, La Jolla, California, USA. [6]Department of Biochemistry, McGill University, Montréal, Quebec, Canada. [7]Division of Developmental Immunology, La Jolla Institute for Allergy and Immunology, La Jolla, California, USA. [8]Clinical Science, Broegelmann Research Laboratory, Bergen, Norway. [9]Department of Microbiology, Jagiellonian University, Krakow, Poland. [10]Laboratory of Experimental Immunology, Immunology Frontier Research Center, Osaka University, Suita, Japan. [11]Department of Experimental Pathology, Institute for Frontier Medical Sciences, Kyoto University, Kyoto, Japan. [12]Monash Biomedicine Discovery Institute, and [13]Department of Biochemistry and Molecular Biology, Monash University, Clayton, Victoria, Australia.

Genetic variants at the *PTPN2* locus, which encodes the tyrosine phosphatase PTPN2, cause reduced gene expression and are linked to rheumatoid arthritis (RA) and other autoimmune diseases. PTPN2 inhibits signaling through the T cell and cytokine receptors, and loss of PTPN2 promotes T cell expansion and CD4- and CD8-driven autoimmunity. However, it remains unknown whether loss of PTPN2 in FoxP3+ regulatory T cells (Tregs) plays a role in autoimmunity. Here we aimed to model human autoimmune-predisposing *PTPN2* variants, the presence of which results in a partial loss of *PTPN2* expression, in mouse models of RA. We identified that reduced expression of *Ptpn2* enhanced the severity of autoimmune arthritis in the T cell–dependent SKG mouse model and demonstrated that this phenotype was mediated through a Treg-intrinsic mechanism. Mechanistically, we found that through dephosphorylation of STAT3, PTPN2 inhibits IL-6–driven pathogenic loss of FoxP3 after Tregs have acquired RORγt expression, at a stage when chromatin accessibility for STAT3-targeted IL-17–associated transcription factors is maximized. We conclude that PTPN2 promotes FoxP3 stability in mouse RORγt+ Tregs and that loss of function of PTPN2 in Tregs contributes to the association between *PTPN2* and autoimmunity.

Introduction

Rheumatoid arthritis (RA) is a chronic autoimmune, systemic inflammatory disorder that primarily affects diarthrodial joints (1). To date, various genome-wide association studies have identified over 100 risk loci for RA (2, 3). One gene found to be highly associated with RA is *PTPN2*, which encodes for the protein tyrosine phosphatase (PTP) PTPN2, also known as T cell PTP (2). PTPN2 also strongly associates with inflammatory bowel disease (4). Homozygous carriage of the risk allele at the rs1893217 SNP — which tags an autoimmunity-associated *PTPN2* haplotype — results in a 33%–50% decrease in *PTPN2* mRNA in human CD4+ memory T cells (5). Also, the same rs1893217 risk allele drove reduced PTPN2 protein expression and acted as a loss-of-function variant when transfected into THP-1 cells (6).

PTPN2 is a ubiquitously expressed PTP, and in hematopoietic cells it works as an important negative regulator of T cell receptor (TCR) and cytokine signaling by dephosphorylating the SRC-family kinases Lck and Fyn, Janus kinase-1 (JAK1) and JAK3, and signal transducer and activator of transcription-1 (STAT1), STAT3, and STAT5 (7–11).

How loss of function of PTPN2 promotes risk of RA and other autoimmune diseases is incompletely understood. However, the importance of PTPN2 in inflammation is exemplified by the fact that global deletion of *Ptpn2* in mice leads to early lethality due to progressive systemic myeloid cell–driven inflammation (12). Further experiments with mice carrying conditional deletion of *Ptpn2* demonstrated that PTPN2 also plays a critical role in maintenance of T cell tolerance. Mice carrying T cell–specific deletion of *Ptpn2* showed enhanced TCR signaling, altered thymic selection, and increased proliferation of peripheral T cells, together resulting in CD8-driven systemic autoimmunity (9). Complete *Ptpn2* deficiency in T cells also favored CD4 polarization toward a Th1 and Th17 fate, promoting aggressive colitis (13), which correlated with increased Th1 and Th17 marker expression in inflamed colon tissue from Crohn's disease patient carriers of rs1893217 (13).

Although these studies point to a role of PTPN2 in modulation of T cell tolerance, it remains unclear how loss of function of PTPN2 affects autoimmunity-protective FoxP3+ regulatory T cells (Tregs) (14, 15). Two studies showing that complete knockout (KO) (9, 10) of *Ptpn2* promotes Treg expansion and FoxP3 stabilization in induced Tregs (16) suggest that loss of function of *Ptpn2* in Tregs might partially counterbalance the autoimmunity

risk induced by *Ptpn2* KO in FoxP3⁻ CD4⁺ and CD8⁺ T cells. However, the role of PTPN2 or other tyrosine phosphatases in Tregs has yet to be addressed through cell-specific genetic manipulation.

In the present study, aimed to model the effect of partial loss of function of *PTPN2* in autoimmunity-prone human carriers, we assessed whether haploinsufficiency of *Ptpn2* enhances severity of disease in multiple models of RA. We show that *Ptpn2* haploinsufficiency promotes CD4-driven autoimmune arthritis. Unexpectedly, we found that partial loss of function of *Ptpn2* in Tregs promotes autoimmunity by destabilizing FoxP3 expression in the context of arthritis-induced inflammation.

Results

PTPN2 haploinsufficiency promotes T cell–mediated arthritis. Figure 1, A–C, shows an in silico assessment of the extent of overlap between RA-associated SNPs and DNase I hypersensitivity sites (DHSs) and active histone marks in the *PTPN2* locus for different immune cell types. This type of analysis is useful for insight about the key cellular players where the *PTPN2* locus selectively harbors a higher number of *cis*-regulatory DNA elements (DHSs) and which are thus most likely to be perturbed by the RA-associated SNPs (17). We found that the *PTPN2* locus shows distinct patterns of DHS and histone modifications in CD4⁺ T cells as compared with B cells and monocytes (Figure 1A and Supplemental Figure 1A and Supplemental Table 1; supplemental material available online with this article; https://doi.org/10.1172/JCI123267DS1), suggesting that the locus is more accessible and active in T cells. CD4⁺ memory T cells were particularly enriched for DHS within the *PTPN2* locus (Figure 1B and Supplemental Table 2). RA-associated *PTPN2* SNPs that directly overlap with DHSs were also enriched in CD4⁺ T cells, overall pointing to CD4⁺ T cells as the key cellular target of *PTPN2*-dependent pathogenesis of RA (Figure 1C and Supplemental Table 3).

Since PTPN2 regulates important functions in innate immune cells such as macrophages and in synovial fibroblasts (7, 18), we first subjected *Ptpn2*⁺/⁺ and *Ptpn2*⁺/⁻ BALB/c mice to K/BxN passive serum transfer and collagen antibody–induced arthritis (CAIA), 2 models dependent on innate immune cells (19–22). In these models, *Ptpn2* haploinsufficiency did not affect development of arthritis (Figure 1D and Supplemental Figure 1, B and C), suggesting that partial loss of function of *Ptpn2* does not enhance the arthritogenic action of innate immune cells.

We next evaluated the effect of *Ptpn2* haploinsufficiency in the SKG model of autoimmune arthritis. The *Zap70^{SKG}* (W163C) mutation results in altered thymic selection and emergence of self-reactive T cells that, in the context of the H-2^d haplotype, result in Th17 cell–dependent spontaneous arthritis (23, 24). Partial loss of function of *Ptpn2* significantly increased spontaneous development of arthritis in female SKG mice (Figure 1E), with increased cartilage depletion and bone damage (Supplemental Figure 1, D and E).

Arthritis onset can be synchronized in SKG mice by injection of mannan (23). Male *Ptpn2*⁺/⁻ SKG mice developed worse arthritis after injection of mannan, correlating with significantly increased expression of the inflammatory cytokines *Il1b*, *Tnf*, *Il6*, *Tnfsf11* (the gene encoding RANK ligand), and *Il17a* in arthritic ankles (Figure 2, A–D). We also observed an increased severity of mannan-induced arthritis in female *Ptpn2*⁺/⁻ SKG mice (data not shown). We conclude that *Ptpn2* haploinsufficiency, which reduces the

expression of *Ptpn2* to levels comparable to what was reported for carriers of disease-associated *PTPN2* SNPs (Supplemental Figure 1F), enhances severity of arthritis in a T cell–mediated but not in an innate immune cell–mediated model of arthritis.

Ptpn2 haploinsufficiency promotes enrichment of Th17 cells and ectopic lymphoid-like structures. Next, we immunophenotyped *Ptpn2*⁺/⁺ and *Ptpn2*⁺/⁻ SKG mice subjected to mannan-induced arthritis. We found no difference in the number of total CD4⁺ T cells or in effector populations Th1 and Th17 or Tregs in popliteal lymph nodes of *Ptpn2*⁺/⁺ versus *Ptpn2*⁺/⁻ SKG mice (Figure 3A).

In SKG arthritic ankles we mainly found CD4⁺ T cells with an effector phenotype (Figure 3B), while, consistent with previous reports, CD8⁺ T cells were almost absent (24, 25). Arthritic joints from *Ptpn2*⁺/⁻ SKG mice displayed increased numbers of CD4⁺ T cells with specific expansion of Th17 cells when compared with arthritic joints from *Ptpn2*⁺/⁺ SKG mice (Figure 3, C–E). There was no difference in the number of either RORγt⁺ or RORγt⁻ Tregs, and no Th1 cells were found within arthritic ankles (Figure 3, D and E). There was a significant correlation between the number of Th17 cells in arthritic ankles and the clinical arthritis score (Figure 3E), suggesting that the arthritogenic action of *Ptpn2* haploinsufficiency in SKG mice is mediated through increased joint accumulation of Th17 cells.

Assessment of synovial tissue from arthritic *Ptpn2*⁺/⁻ SKG mice also displayed an increased presence of lymphoid nodules composed by B cells (B220⁺), clustering within close proximity to CD4⁺ T cells (Figure 3, F and G). The formation of these lymphoid nodules was reminiscent of the ectopic lymphoid structures (ELSs) that are present within the synovium of a subgroup of RA patients and correlate with more severe disease course (26). Th17 cells can contribute to the formation of ELS through production of IL-17, which stimulates expression of CXCL13 (26, 27). Consistent with the increased accumulation of Th17 cells in *Ptpn2*⁺/⁻ SKG arthritic ankles, we found an increased expression of ELS-associated genes including *Cxcl12*, *Cxcl13*, *Lta*, *Ltb*, and *Prdm1* (28) in the same joints (Figure 3H), while there was no difference in the expression of *Bcl6*. Together, these results further support the notion that increased arthritis in *Ptpn2*⁺/⁻ SKG mice is mediated through a Th17-dependent mechanism.

T cell–specific haploinsufficiency of Ptpn2 promotes arthritis. Previous studies have concluded that B cells play a minor role, if any, in SKG arthritis (24). Accordingly, B cell depletion during the arthritic phase did not influence disease severity in SKG mice (Supplemental Figure 2); thus it is unlikely that promotion of SKG arthritis by *Ptpn2* haploinsufficiency is mediated through an action on B cells.

We therefore turned our attention to T cells. To verify that the partial loss of function of *Ptpn2* promotes SKG arthritis through a T cell–intrinsic mechanism, we generated SKG mice carrying T cell–specific haploinsufficiency of *Ptpn2* on the B6 background. First, we backcrossed the SKG mutation onto the B6 background for 10 generations. Next, we made our B6.SKG mice congenic for the H2^d haplotype, thus generating B6.SKG.H2^{d/d} mice. We verified that B6.SKG.H2^{d/d} mice developed arthritis similar to that of SKG mice after injection of mannan, and displayed similar synovial inflammation and bone destruction (Figure 4, A and B). Also, B6.SKG.H2^{d/d} mice showed enrichment of Th17 cells in popliteal lymph nodes and arthritic ankles similar to that seen in SKG mice (Figure 4C).
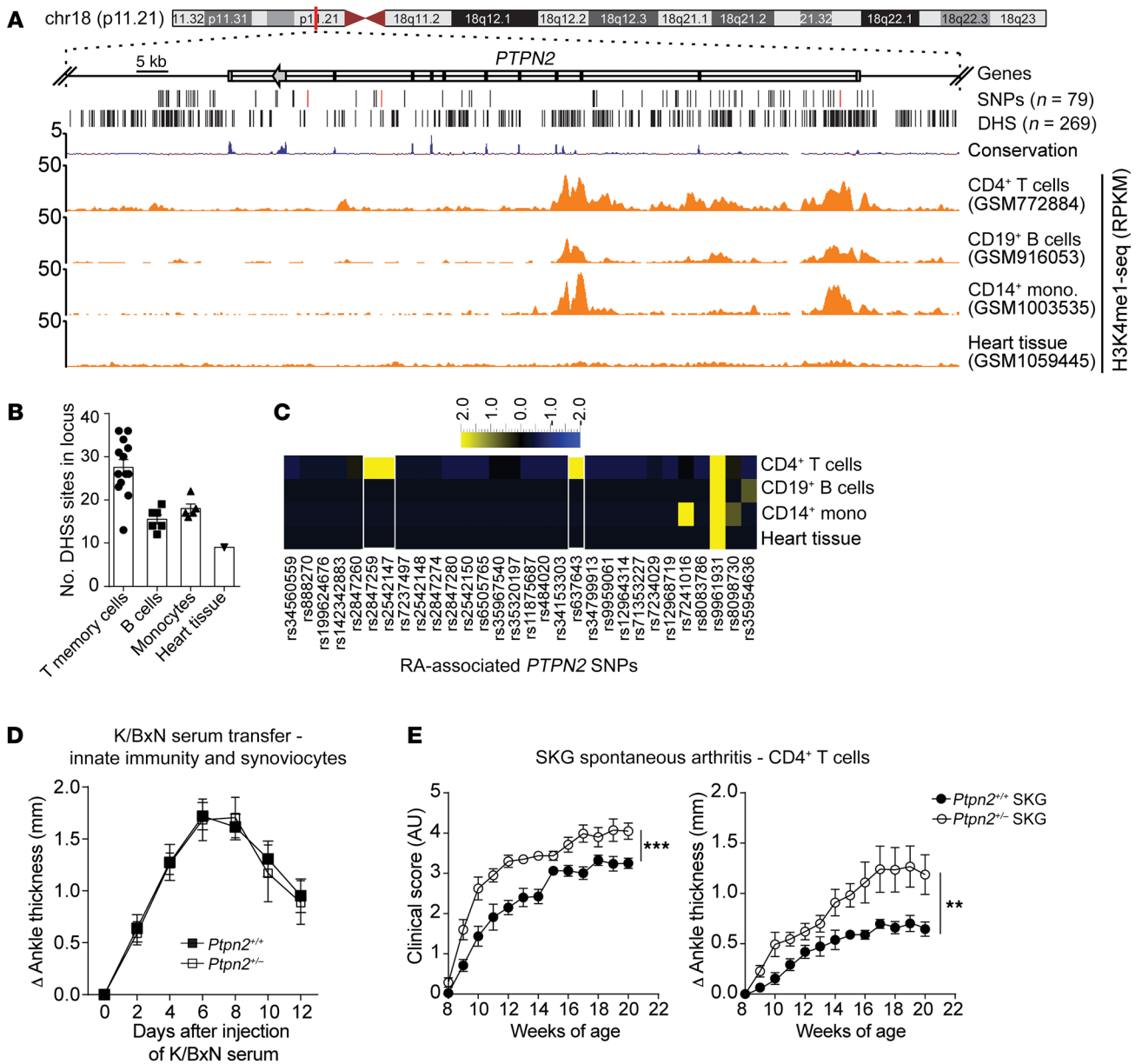
Figure 1. RA-associated haploinsufficiency of *Ptpn2* promotes T cell–dependent arthritis in mice. (**A**) UCSC tracks showing the chromosomal location of the human *PTPN2* gene, containing a large haplotype block of RA-associated SNPs. Black lines indicate SNPs' genomic location (the characterizing SNPs rs2847297, rs1893217, and rs8083786 are indicated in red), and DNase hypersensitivity sites (DHSs). Example tracks of H3K4me1-seq from CD4+ T cells, CD19+ B cells, CD14+ monocytes, and heart tissue. RPKM, reads per kilobase of transcript per million mapped reads. (**B**) Number of DHSs in the *PTPN2* locus in single data sets of 4 primary cell types. (**C**) Heatmap of RA-associated SNPs (columns) that overlap with DHSs in different primary cell types (rows). (**D**) Development of K/BxN serum-induced arthritis in *Ptpn2*+/+ (*n* = 9) and *Ptpn2*+/− (*n* = 7) male BALB/c mice. (**E**) Clinical score and ankle thickness during development of spontaneous arthritis in female *Ptpn2*+/+ (*n* = 8) and *Ptpn2*+/− (*n* = 8) SKG mice. Compiled data from at least 2 independent experiments are shown in **D** and **E**. Arthritis severity was quantified using the area under the curve. Bars represent mean ± SEM. **P < 0.01, ***P < 0.001 by Mann-Whitney.

B6.SKG.H2$^{d/d}$ mice were further crossed with *Ptpn2*-floxed (*Ptpn2*$^{fl/fl}$) and Lck-Cre+ mice, thus generating B6.SKG.H2$^{d/d}$. *Ptpn2*$^{fl/+}$.Lck-Cre+ mice carrying T cell–specific haploinsufficiency of *Ptpn2* (Figure 4D). When subjected to mannan-induced arthritis, female and male B6.SKG.H2$^{d/d}$.*Ptpn2*$^{fl/+}$.Lck-Cre+ mice displayed more severe disease compared with control B6.SKG. H2$^{d/d}$.*Ptpn2*$^{fl/+}$.Lck-Cre− mice (Figure 4, E and F). We conclude that *Ptpn2* haploinsufficiency promotes development of SKG arthritis through an intrinsic effect on T cells.

Ptpn2-haploinsufficient CD4+ T cells transfer enhanced arthritis severity. SKG CD4+ T cells can transfer arthritis to Rag2-KO mice (23). As shown in Figure 5, A–C, Rag2-KO mice transferred with CD4+ T cells isolated from *Ptpn2*+/− SKG mice developed significantly worse arthritis than mice transferred with CD4+ T cells from *Ptpn2*+/+ SKG mice. Importantly, transfer of *Ptpn2*+/− SKG CD4+ T cells also caused increased formation of lymphoid nodules in arthritic ankles of Rag2-KO mice (Figure 5D). These data confirm that *Ptpn2* haploinsufficiency enhances arthritis through an action on CD4+ T cells.
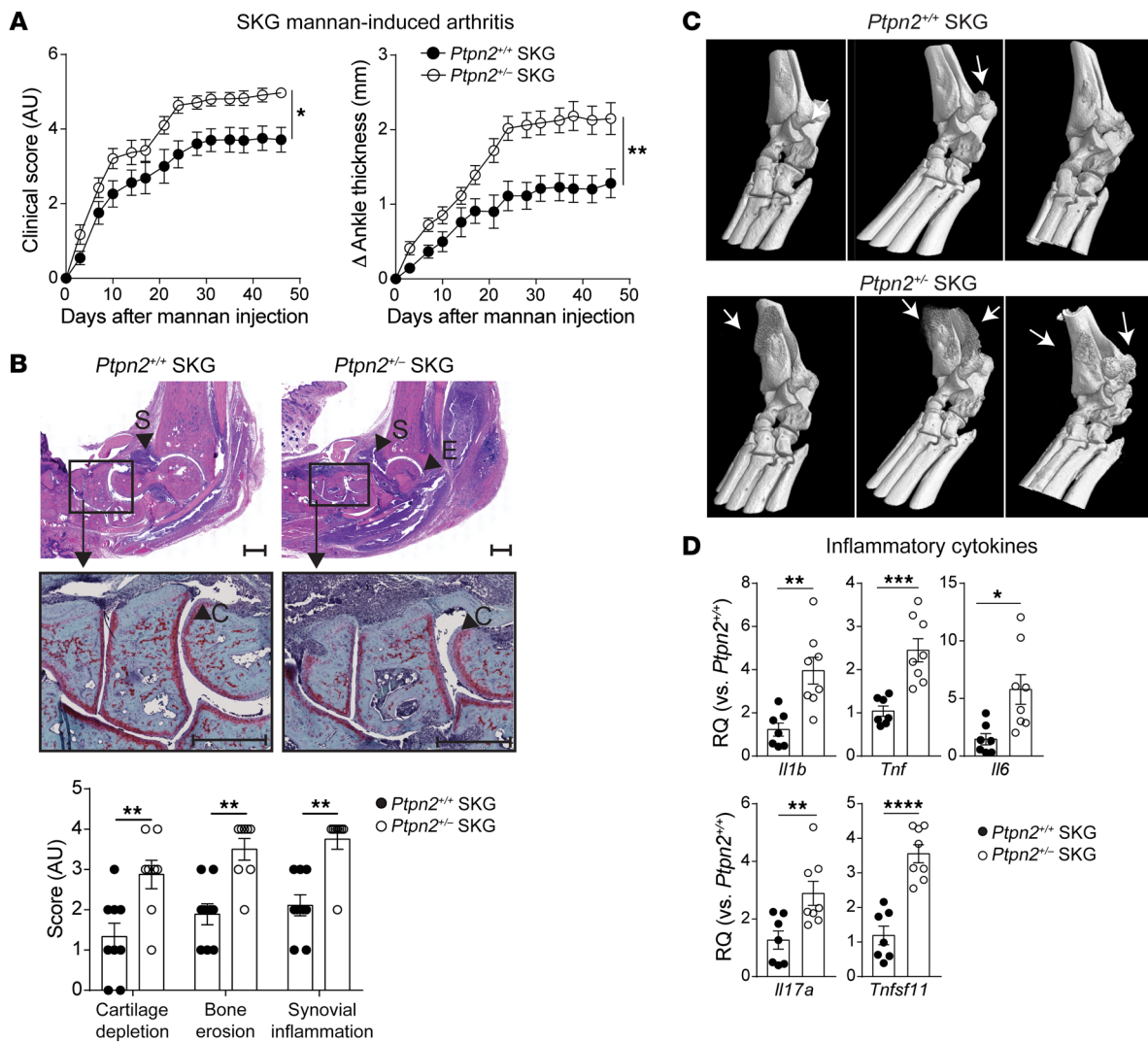
Figure 2. *Ptpn2* haploinsufficiency aggravates mannan-induced arthritis in SKG mice. (**A**) Clinical score and ankle thickness in male *Ptpn2*⁺/⁺ (*n* = 13) and *Ptpn2*⁺/⁻ (*n* = 11) SKG mice after mannan injection. (**B**) Representative images of H&E (top panels) and safranin-O staining (middle panels) of ankles from *Ptpn2*⁺/⁺ (*n* = 9) and *Ptpn2*⁺/⁻ (*n* = 8) SKG mice with mannan-induced arthritis. Arrowheads indicate synovial inflammation (S), bone erosion (E), and cartilage depletion (C), which are quantified in the lower panel. Scale bars: 500 μm. (**C**) Micro-CT of arthritic ankles from individual *Ptpn2*⁺/⁺ and *Ptpn2*⁺/⁻ male SKG mice with mannan-induced arthritis. Arrows indicate bone erosion or reactive bone deposition that is markedly increased in *Ptpn2*⁺/⁻ SKG mice. (**D**) Quantitative PCR analysis of cytokine gene expression in ankles of *Ptpn2*⁺/⁺ (*n* = 7) and *Ptpn2*⁺/⁻ (*n* = 8) male SKG mice 35 days after mannan injection. RQ, relative quantification. Compiled data from at least 2 independent experiments are shown in **A**–**D**. Arthritis severity was quantified using the area under the curve. Each symbol in **B** and **D** represents an individual mouse. Bars represent mean ± SEM. *P < 0.05, **P < 0.01, ***P < 0.001, ****P < 0.0001 by Mann-Whitney (**A** and **B**) or unpaired *t* test (**D**).

In order to understand how *Ptpn2* haploinsufficiency affects CD4⁺ T cell differentiation during SKG arthritis, we generated CD4⁺ T cell chimeras by transferring CD4⁺ T cells isolated from prearthritic CD45.1 and CD45.2 *Ptpn2*⁺/⁺ or *Ptpn2*⁺/⁻ SKG mice into Rag2-KO mice (Figure 5E). Assessment of arthritic chimeric mice revealed preferential expansion of *Ptpn2*⁺/⁻ SKG CD4⁺ T cells over *Ptpn2*⁺/⁺ SKG CD4⁺ T cells in lymph nodes (Figure 5F). We observed preferential expansion of *Ptpn2*⁺/⁻ SKG Tregs in the spleen and of Th1 and especially Th17 cells in lymph nodes (Figure 5, G and H). The above-mentioned phenotype was not due to differences in the frequencies of naive or effector subsets of CD4⁺ T cells in the prearthritic mice used for adoptive transfer (Supplemental Figure 3A). We conclude that *Ptpn2* haploinsufficiency leads to increased expansion of SKG CD4⁺ T cells and their effector subsets after transfer into lymphopenic hosts.

Thymic selection and TCR signaling are not altered by Ptpn2 haploinsufficiency. Complete deletion of *Ptpn2* in T cells alters thymic selection and promotes peripheral expansion of specific T cell clones, effects that depend on the role of PTPN2 as a negative regulator of TCR signaling (9, 10, 29). However, we did not find any evidence for altered thymic selection or selective expansion of specific peripheral Vβ CD4⁺ T cell clones in *Ptpn2*⁺/⁻ SKG mice compared with *Ptpn2*⁺/⁺ SKG mice (Supplemental Figure 3, B and C). Also, we did not detect any differences in the induction of CD69 or CD25 after TCR stimulation between *Ptpn2*⁺/⁺ and *Ptpn2*⁺/⁻ naive SKG CD4⁺ T cells (Supplemental Figure 4, A and B).
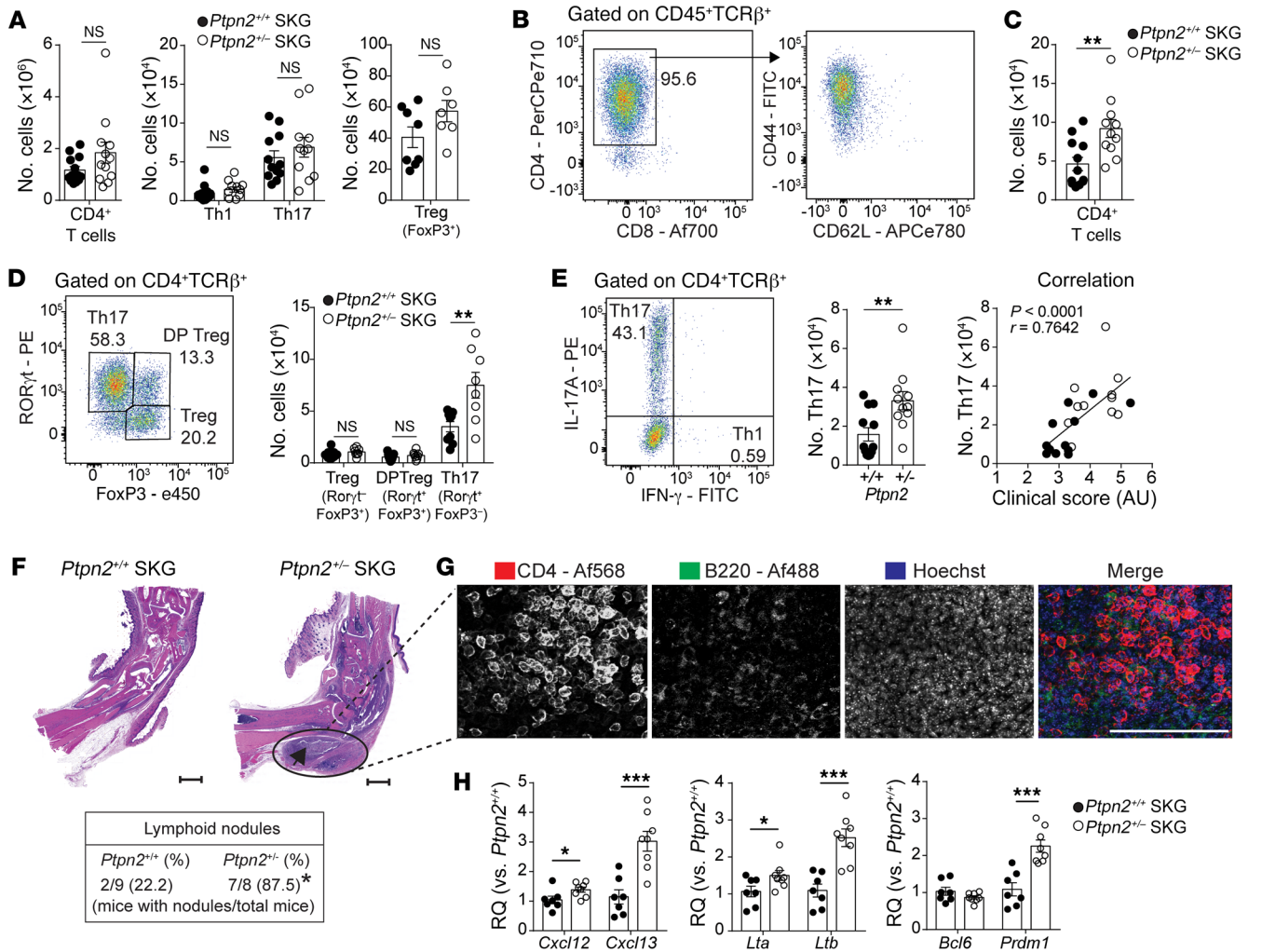
Figure 3. Increased accumulation of synovial Th17 cells and ELSs in *Ptpn2*-haploinsufficient SKG mice. (**A**) Number of CD4⁺ T cells and effector populations Th1 and Th17 (*Ptpn2*⁺/⁺, *n* = 12; *Ptpn2*⁺/⁻, *n* = 11) and Tregs (*Ptpn2*⁺/⁺, *n* = 8; *Ptpn2*⁺/⁻, *n* = 7) in popliteal lymph nodes of SKG mice 30–35 days after mannan injection. (**B**) Distribution of CD4⁺ and CD8⁺ T cells among TCRβ⁺ T cells (left) and expression of CD44 and CD62L on CD4⁺ T cells (right) in arthritic ankles after mannan injection. (**C** and **D**) Number of CD4⁺ T cells in arthritic ankles and Tregs (TCRβ⁺CD4⁺FoxP3⁺RORγt⁻), RORγt⁺ Tregs (TCRβ⁺CD4⁺FoxP3⁺ RORγt⁺), and Th17 cells (TCRβ⁺CD4⁺FoxP3⁻RORγt⁺) in ankles of *Ptpn2*⁺/⁺ (*n* = 9) and *Ptpn2*⁺/⁻ (*n* = 8) male SKG mice 30–35 days after mannan injection. (**E**) Number of Th17 cells (TCRβ⁺CD4⁺IL-17A⁺IFN-γ⁻; left) and the correlation between clinical score and number of Th17 cells within ankles (right; Spearman correlation) of male *Ptpn2*⁺/⁺ (*n* = 12, black circles) and *Ptpn2*⁺/⁻ (*n* = 11, white circles) SKG mice 30–35 days after mannan injection. (**F**) Representative microscopic images used to assess the presence of ELSs (black arrow; scale bars: 500 μm) in male *Ptpn2*⁺/⁺ and *Ptpn2*⁺/⁻ SKG mice after mannan injection (*P = 0.015, Fisher's exact test). (**G**) Representative 2-dimensional maximum-intensity projection of multipanel confocal images of CD4 (red) and B220 (green) in ELSs from ankle synovial tissue of male *Ptpn2*⁺/⁻ SKG mice 35 days after mannan injection. Representative of 3 individual mice. Scale bar: 200 μm. (**H**) Quantitative PCR analysis of ELS-associated gene expression in ankles of male *Ptpn2*⁺/⁺ (*n* = 7) and *Ptpn2*⁺/⁻ (*n* = 8) SKG mice 35 days after mannan injection. Compiled data from at least 2 independent experiments are shown in **A–H**. Each symbol in **A–E** and **H** represents an individual mouse. Bars represent mean ± SEM. *P < 0.05, **P < 0.01, ***P < 0.001 by unpaired *t* test.

Although further studies are needed to conclusively rule out a role for *Ptpn2* haploinsufficiency in thymic selection, our data strongly suggest that *Ptpn2* haploinsufficiency promotes arthritis development through peripheral expansion of pathogenic Th17 and perhaps also Th1 cells.

Increased sensitivity to IL-2 in Ptpn2-haploinsufficient CD4⁺ T cells. Although an expansion of *Ptpn2*⁺/⁻ Th1 cells was only observed in T cell–chimeric mice and not in arthritic *Ptpn2*⁺/⁻ SKG mice, we did consider a potential arthritogenic role of *Ptpn2*-haploinsufficient Th1 cells. Since IL-2 promotes differentiation of Th1 cells (30) and previous reports have identified PTPN2 as an important

negative regulator of IL-2 signaling in CD4⁺ T cells (9), we first assessed IL-2 signaling in preactivated *Ptpn2*⁺/⁺ versus *Ptpn2*⁺/⁻ naive SKG CD4⁺ T cells. In line with previous reports, we found increased IL-2–induced activation of STAT5 in naive *Ptpn2*⁺/⁻ SKG CD4⁺ T cells (Supplemental Figure 4C). This enhanced sensitivity to IL-2 correlated with significantly increased differentiation into Th1 cells from naive *Ptpn2*⁺/⁻ SKG CD4⁺ T cells, while there was no evidence of enhanced IFN-γ signaling (Supplemental Figure 4, D and E). However, IFN-γ–producing SKG CD4⁺ T cells, i.e., Th1 cells, play a protective role in SKG arthritis (31). Accordingly, global KO of IFN-γ aggravated arthritis development in SKG mice (Sup-
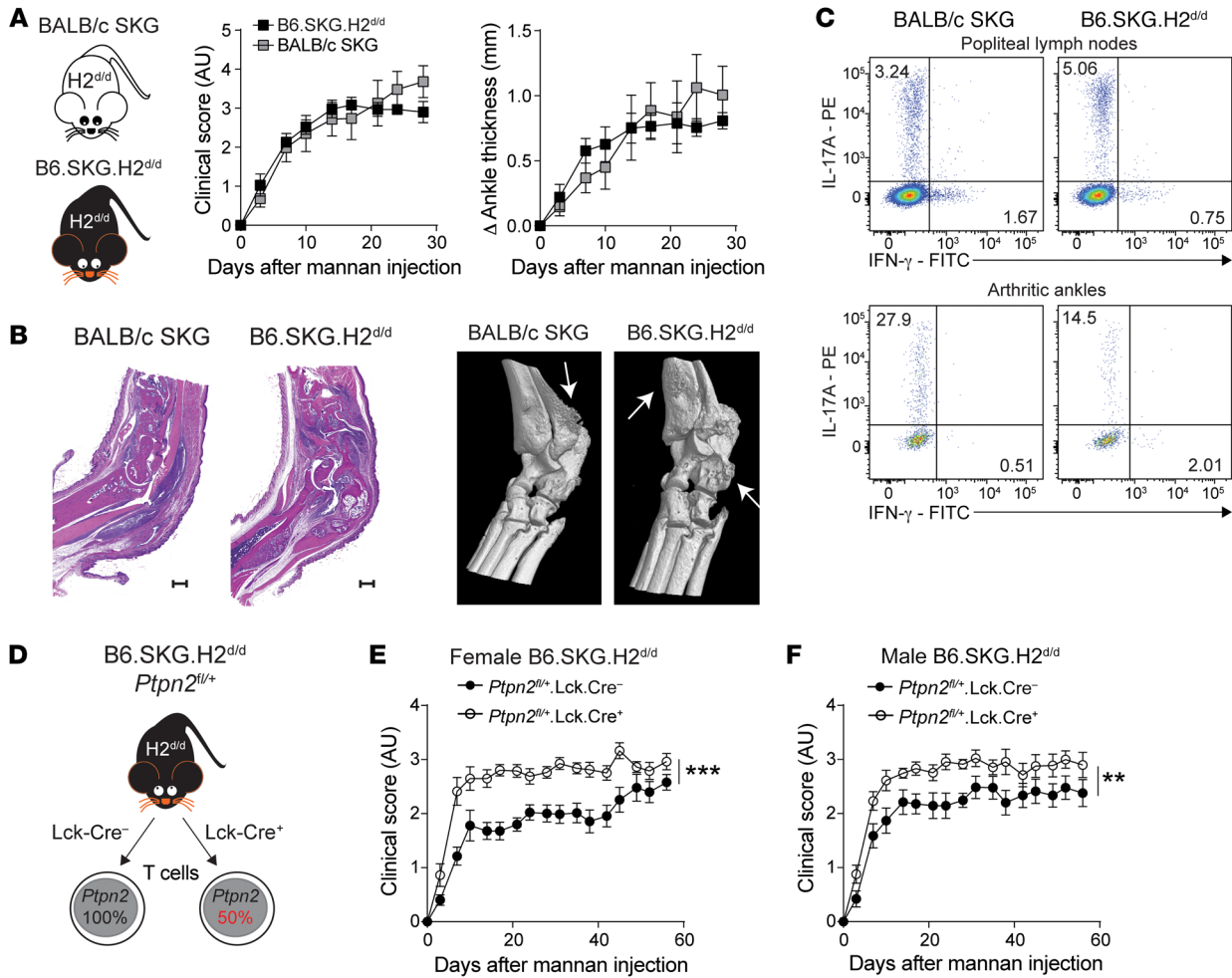
Figure 4. *Ptpn2* haploinsufficiency promotes arthritis through T cells. (**A**) Clinical score and ankle swelling in BALB/c SKG (*n* = 6) and B6.SKG.H2^d/d (*n* = 6) mice after injection of mannan. (**B**) Representative H&E staining (left; scale bars: 500 μm) and representative micro-CT images (right) of arthritic ankles from BALB/c SKG and B6.SKG.H2^d/d mice. Arrows indicate bone erosion or reactive bone deposition. (**C**) Representative flow cytometry staining of Th1 and Th17 in popliteal lymph nodes (top) and arthritic ankles (bottom) of BALB/c SKG and B6.SKG.H2^d/d mice. (**D**) Generation of B6.SKG.H2^d/d mice with a T cell–specific haploinsufficiency of *Ptpn2*. (**E** and **F**) Clinical score of mannan-induced arthritis in female (**E**) and male (**F**) B6.SKG.H2^d/d*Ptpn2*^fl/+Lck-Cre^− (female, *n* = 9; male, *n* = 9) and B6.SKG.H2^d/d*Ptpn2*^fl/+Lck-Cre^+ (female, *n* = 8; male, *n* = 9) mice. Compiled data from at least 2 independent experiments are presented. Arthritis severity was quantified using the area under the curve. Bars represent mean ± SEM. **P < 0.01, ***P < 0.001 by Mann-Whitney.

plemental Figure 4F). We conclude that although increased IL-2 signaling in *Ptpn2*^+/− SKG mice can promote Th1 (and potentially Treg) expansion, Th1 cells are unlikely to mediate the increased arthritis severity observed in these mice.

Enhanced arthritis is driven by IL-6 and IL-17. Development of arthritis in SKG mice is partially dependent on IL-6 and IL-17 (23, 25, 31). We verified the IL-17–dependence of SKG arthritis and lymphoid nodule development by treating SKG and SKG CD4^+ T cell–recipient Rag2-KO mice with IL-17A–neutralizing antibodies during the course of mannan-induced arthritis (Supplemental Figure 5, A–D). To determine whether enhanced arthritis in *Ptpn2*^+/− SKG mice was IL-17– and/or IL-6–dependent, we treated *Ptpn2*^+/+ and *Ptpn2*^+/− SKG mice with IL-17A–neutralizing or IL-6 receptor–blocking (IL-6R–blocking) antibodies. Both treatments eliminated differences in arthritis development and lymphocyte accumulation in arthritic ankles between *Ptpn2*^+/+ and *Ptpn2*^+/− SKG mice (Figure 6, A–C), while only partially suppressing disease devel-

opment. Another cytokine that is important for the pathogenesis of arthritis in SKG mice is TNF-α (25). However, we did not find any difference in TNF-α production between *Ptpn2*^+/+ and *Ptpn2*^+/− SKG CD4^+ T cells (Supplemental Figure 5E). These data suggest that the increased arthritis in *Ptpn2*^+/− SKG mice is driven by IL-6 and IL-17 but not by increased TNF-α production from CD4^+ T cells. We only detected minimal IL-6 production from SKG CD4^+ T cells, which was unaffected by *Ptpn2* haploinsufficiency (Supplemental Figure 5, F and G), pointing to T cell–extrinsic sources of IL-6 as critical for the enhanced arthritis of *Ptpn2*^+/− SKG mice.

PTPN2 haploinsufficiency promotes conversion of Tregs. IL-6 is required for the differentiation of naive CD4^+ T cells into Th17 (32). In contrast to previous reports showing that complete loss of *Ptpn2* promotes Th17 differentiation (13), naive SKG CD4^+ T cells from *Ptpn2*^+/− mice did not display enhanced capacity for Th17 differentiation in vitro (Figure 6D). This was not due to an altered expression of the *il6r* complex in *Ptpn2*^+/− naive SKG CD4^+
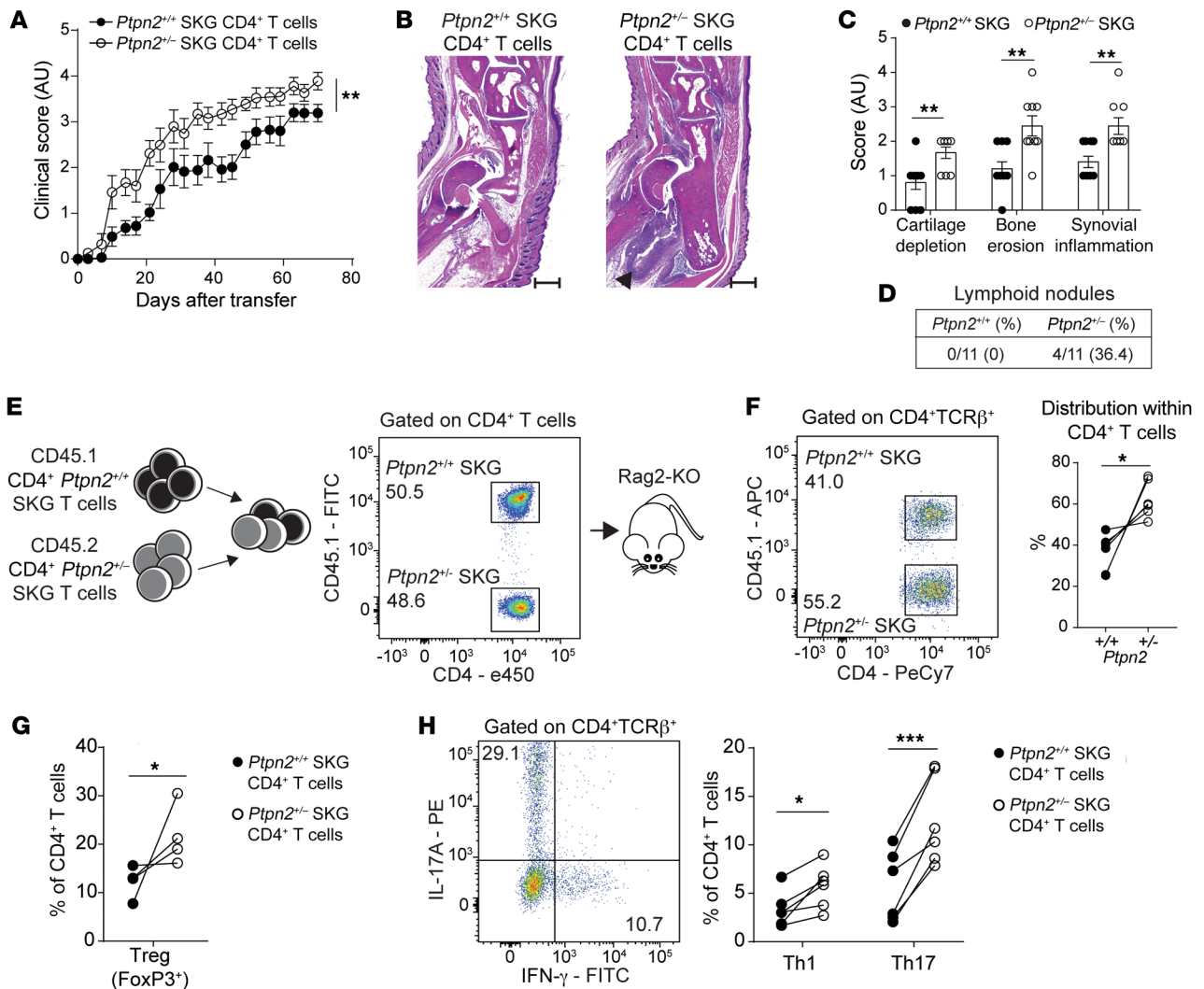
Figure 5. *Ptpn2*-haploinsufficient CD4⁺ T cells transfer enhanced arthritis to Rag2-KO mice. (A) Clinical scores after transfer of total CD4⁺ SKG T cells isolated from prearthritic *Ptpn2*⁺/⁺ (*n* = 10) and *Ptpn2*⁺/⁻ (*n* = 10) male SKG mice to male Rag2-KO mice. (**B** and **C**) Representative H&E staining used for histological evaluation (**B**; scale bar: 500 μm; quantification shown in **C**) of ankle joints of Rag2-KO mice in **A** (*n* = 10 for each genotype). (**D**) Presence of ELSs in arthritic ankles of Rag2-KO mice after transfer with CD4⁺ SKG T cells in **A**. (**E**) Generation of CD4⁺ SKG T cell chimeras. (**F–H**) Analysis of expansion of CD4⁺ T cells (**F**; *n* = 6) and effector populations Th1 and Th17 in lymph nodes (**H**; *n* = 6) and Tregs in the spleen (**G**; *n* = 4) of T cell chimeras during the arthritic phase (12–14 weeks after transfer) in Rag2-KO mice. Compiled data from at least 2 independent experiments are presented. Each symbol in **C–H** represents an individual mouse. Arthritis severity was quantified using the area under the curve. Bars represent mean ± SEM. *P < 0.05, **P < 0.01, ***P < 0.001 by Mann-Whitney (**A** and **C**) or paired *t* test (**F–H**).

T cells (Supplemental Figure 5H). Thus, the accumulation of Th17 observed in arthritic joints of *Ptpn2*⁺/⁻ SKG mice is unlikely to be due to increased differentiation of naive CD4⁺ T cells into Th17.

IL-6–dependent conversion of FoxP3⁺ Tregs into IL-17–producing FoxP3⁻ T cells has previously been reported in the collagen-induced arthritis (CIA) model, and suggested as a source of autoreactive IL-17–producing cells in RA (33). We therefore questioned whether *Ptpn2* haploinsufficiency promotes IL-6–dependent loss of FoxP3 by Tregs and transdifferentiation into IL-17–producing T cells in SKG mice. Figure 6E shows that *Ptpn2*⁺/⁻ SKG Tregs displayed enhanced IL-6–induced in vitro conversion into IL-17–producing FoxP3⁻ cells. Similarly to naive SKG CD4⁺ T cells, *Ptpn2*⁺/⁻ SKG Tregs did not show any change in *Il6r* expression (Supplemental Figure 5H). Next, we assessed the stability of SKG

Tregs during arthritis in vivo by cotransferring CD45.2 SKG CD4⁺ FoxP3⁺ Tregs with CD45.1 SKG CD4⁺CD25⁻ T cells to Rag2-KO mice and subjecting recipient mice to mannan-induced arthritis (Supplemental Figure 5, I and J). We found that during arthritis, *Ptpn2*-haploinsufficient Tregs displayed significantly increased conversion into FoxP3⁻ IL-17A–producing cells (exTregs; Figure 6F). These data point to a role of PTPN2 as a regulator of Treg stability during autoimmune inflammation.

Treg-specific Ptpn2 haploinsufficiency promotes SKG arthritis. To further assess how *Ptpn2* haploinsufficiency influences Treg function during arthritis, we generated a Treg fate-mapping SKG mouse model by crossing B6.SKG.H2^d/d.FoxP3^YFP-Cre mice with B6.SKG.H2^d/d.ROSA-26-tdTomato reporter mice and B6.SKG.H2^d/d.*Ptpn2*^fl/+ mice. The resulting mice (B6.SKG.H2^d/d.FoxP3^YFP-Cre+/−.
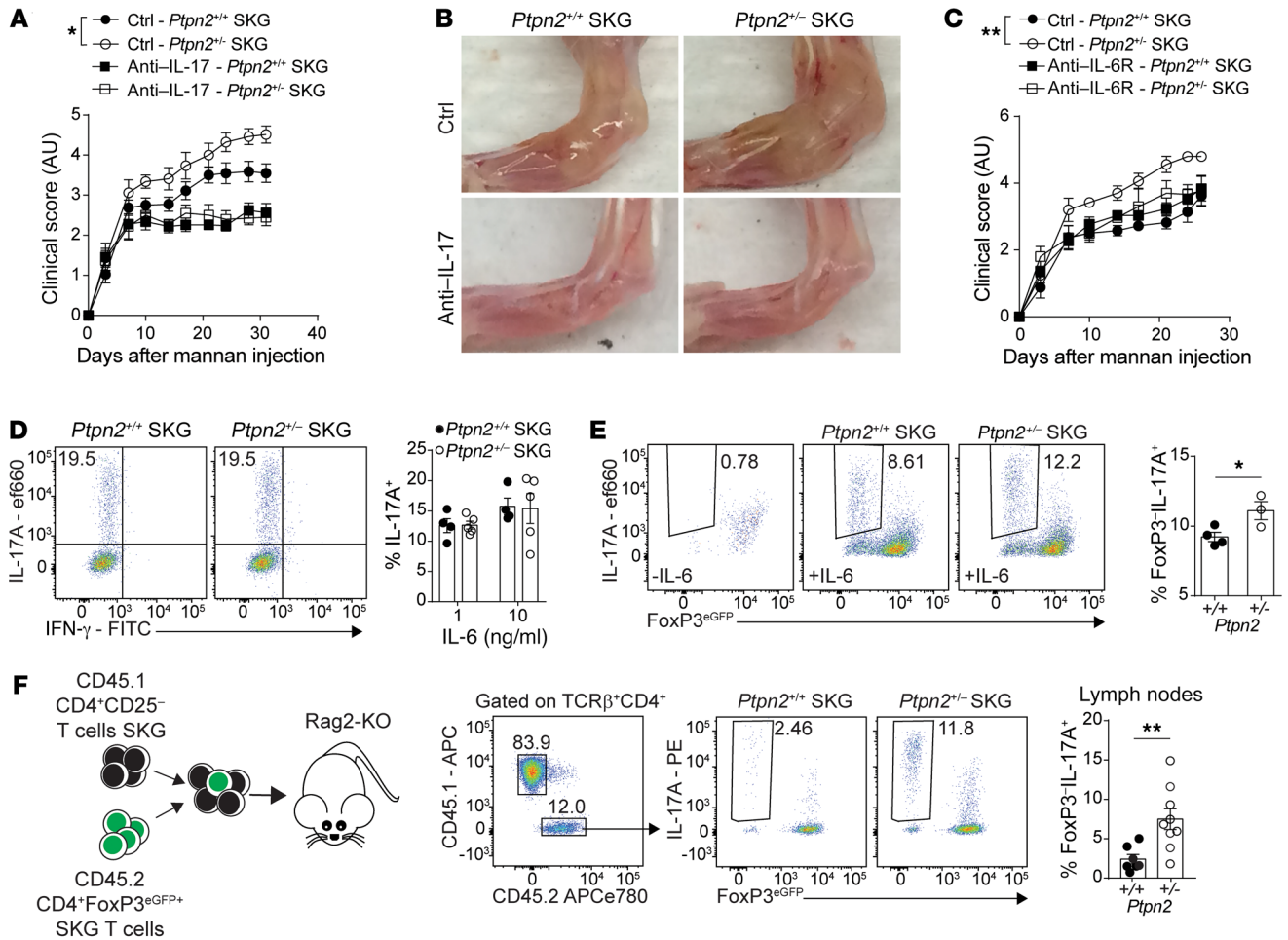
Figure 6. IL-6 promotes arthritis and Treg conversion in *Ptpn2*-haploinsufficient mice. (**A**) Clinical score of male SKG mice after treatment with anti–IL-17A antibodies once weekly (100 μg i.p.; *Ptpn2*+/+, n = 5; *Ptpn2*+/–, n = 4) or control (*Ptpn2*+/+, n = 8; *Ptpn2*+/–, n = 8) during mannan-induced arthritis. (**B**) Representative images of ankles of 4 individual *Ptpn2*+/+ and *Ptpn2*+/– SKG mice treated with anti–IL-17A or control. (**C**) Clinical scores of male *Ptpn2*+/+ and *Ptpn2*+/– SKG mice treated with anti–IL-6R antibody once weekly (200 μg i.p.; *Ptpn2*+/+, n = 3; *Ptpn2*+/–, n = 3) or control (*Ptpn2*+/+, n = 5; *Ptpn2*+/–, n = 5) during mannan-induced arthritis. (**D**) In vitro differentiation of Th17 cells from naive *Ptpn2*+/+ (n = 4) and *Ptpn2*+/– (n = 5) SKG CD4+ T cells. (**E**) Conversion of flow-sorted *Ptpn2*+/+ (n = 4) and *Ptpn2*+/– (n = 3) SKG Tregs (CD4+FoxP3eGFP+) into IL-17–producing exTregs (IL-17A+FoxP3eGFP–) after 72 hours of stimulation with IL-6 (50 ng/ml) and anti-CD3/CD28–coated beads in vitro. (**F**) Cotransfer of CD45.1 SKG CD4+CD25– T cells with CD45.2 SKG Tregs to Rag2-KO mice. Transferred CD45.2 *Ptpn2*+/+ (n = 7) and *Ptpn2*+/– (n = 9) SKG Tregs were analyzed in lymph nodes of arthritic mice. Compiled data from at least 2 independent experiments are shown. Each symbol in **D**–**F** represents an individual mouse. Arthritis severity was quantified using the area under the curve. Bars represent mean ± SEM. *P < 0.05, **P < 0.01 by Mann-Whitney (**A** and **C**) or unpaired t test (**E** and **F**).

tdTomfl/+.*Ptpn2*fl/+ or +/+; Figure 7A) carry Treg-specific haploinsufficiency of *Ptpn2*, in which YFP identifies cells currently expressing FoxP3 (Tregs), whereas tdTomato marks cells that are expressing (Tregs) or did express FoxP3 (exTregs). When subjected to mannan-induced arthritis, we found that female mice carrying Treg-specific haploinsufficiency of *Ptpn2* displayed enhanced arthritis severity (Figure 7B). *Ptpn2*-haploinsufficient Tregs did not display reduced suppressive functions (Supplemental Figure 6, A and B), consistent with previous data from complete-KO Tregs (9). Instead, increased arthritis in mice carrying Treg-specific *Ptpn2* haploinsufficiency correlated with increased frequencies of IL-17–producing exTregs in both joint-draining lymph nodes and arthritic ankles (Figure 7C). Importantly, frequencies of Th17 (YFP–IL-17+IFN-γ–tdTom– CD4+) in the lymph nodes and joints were unaffected by haploinsufficiency of *Ptpn2* in Tregs (Figure

7D). Transfer of in vitro–generated exTregs to Rag2-KO mice was sufficient to induce arthritis, and transfer of *Ptpn2*+/– exTregs led to a faster onset and more severe arthritis compared with transfer of *Ptpn2*+/+ exTregs (Figure 7E). We conclude that *Ptpn2* haploinsufficiency promotes arthritis at least in part at the Treg level, by rendering Tregs more susceptible to FoxP3 loss and conversion into IL-17–producing arthritogenic exTregs.

Expression profile of exTregs is distinct from that of Tregs. To further characterize IL-17+ exTregs and their relationship to Tregs, we performed RNA-Seq on exTregs and Tregs sorted from arthritic Treg fate-mapping mice (Supplemental Figure 6C). We identified around 1820 differentially expressed genes (DEGs; fold change > 2, adjusted P value < 0.05) between Tregs and exTregs (Figure 8A). Several Th17-associated genes (e.g., *Il17a*, *Rorc*, *Il22*, *Il23r*) were found to be upregulated in exTregs, whereas several
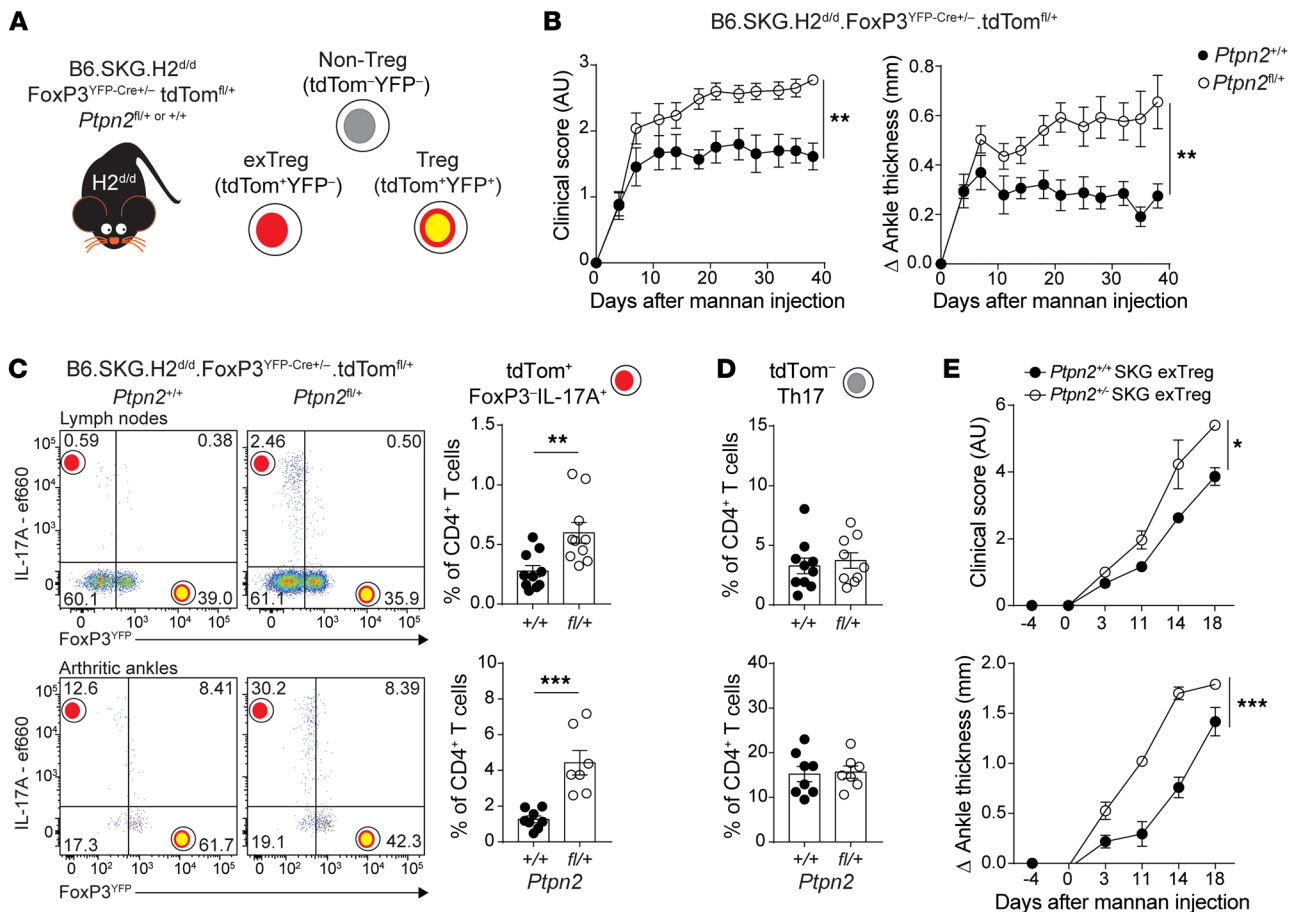
Figure 7. Treg-specific *Ptpn2* haploinsufficiency promotes pathogenic Treg conversion and enhances arthritis severity. (**A**) Generation of B6.SKG.H2$^{d/d}$. FoxP3$^{YFP-Cre+/-}$.tdTom$^{fl/+}$.*Ptpn2$^{fl/+}$* fate-mapping mice. (**B**) Clinical score and ankle swelling of female B6.SKG.H2$^{d/d}$.FoxP3$^{YFP-Cre+/-}$.tdTom$^{fl/+}$.*Ptpn2$^{+/+}$* (*n* = 8) and *Ptpn2$^{fl/+}$* (*n* = 8) mice after injection with mannan at 8 weeks of age. (**C**) IL-17–expressing cells within TCRβ$^+$CD4$^+$tdTom$^+$ cells in lymph nodes (top; axillary and popliteal; *Ptpn2$^{+/+}$*, *n* = 10; *Ptpn2$^{fl/+}$*, *n* = 10) and arthritic ankles (bottom; *Ptpn2$^{+/+}$*, *n* = 8; *Ptpn2$^{fl/+}$*, *n* = 7). Flow plots represent frequency within the TCRβ$^+$CD4$^+$tdTom$^+$ population. Graphs represent frequency within the total TCRβ$^+$CD4$^+$ T cell population. (**D**) Frequency of TCRβ$^+$CD4$^+$tdTom$^-$ Th17 cells represented as the frequency within the total TCRβ$^+$CD4$^+$ T cell population in the same mice as in **C**. (**E**) Transfer of in vitro–generated *Ptpn2$^{+/+}$* (*n* = 3) and *Ptpn2$^{+/-}$* SKG (*n* = 3) eGFP$^-$ exTregs to female Rag2-KO mice (1.5 × 10^5 exTregs per mouse). Arthritis was induced 4 days after transfer by mannan injection. Compiled data from at least 3 independent experiments are presented in **B–D**. Experiment in **E** was performed once. Each symbol in **C** and **D** represents an individual mouse. Arthritis severity was quantified using the area under the curve. Bars represent mean ± SEM. **P* < 0.05, ***P* < 0.01, ****P* < 0.001 by Mann-Whitney (**B**) or unpaired *t* test (**C** and **E**).

Treg-associated genes (e.g., *Foxp3*, *Ctla4*, *Grzmb*, *Gpr83*) were downregulated in exTregs (Figure 8A). Gene expression clustering (fold difference > 2, adjusted *P* value < 0.05) confirmed highly differential transcriptional patterns between exTregs and Tregs, indicating that exTregs represent a unique population that has lost its Treg identity (Figure 8, B and C). IL-17$^+$ exTregs also expressed several genes important for homing to synovial tissue and RA pathogenesis, e.g., *Cxcr6*, *Ccr6*, *Ccl20*, and *Tnfsf11* (Figure 8, A–C). Interestingly, a comparison of gene expression between *Ptpn2$^{fl/+}$* and *Ptpn2$^{+/+}$* exTregs did not reveal any difference (Figure 8D), suggesting that PTPN2 is an upstream regulator of pathways that control Treg stability rather than skewing specific transcriptional patterns in exTregs.

In vitro–generated exTregs recapitulate in vivo exTregs. We next sought to assess whether the exTregs generated in our in vitro conversion assay displayed sufficient similarities to the exTregs found in vivo to enable mechanistic studies of the role of PTPN2 in Treg

stability. RNA-Seq was performed on IL-17A$^+$ exTregs and IL-17A$^-$ Tregs isolated after 72 hours of in vitro conversion assay using Tregs from *Ptpn2$^{+/+}$* and *Ptpn2$^{+/-}$* FoxP3^{eGFP} SKG mice (Supplemental Figure 7A). Gene expression clustering revealed separated genetic expression profiles between Tregs and in vitro–generated exTregs (Figure 9A). We identified around 870 DEGs (fold change > 2, adjusted *P* value < 0.05) between Tregs and in vitro–generated exTregs (Supplemental Figure 7B). Although in vitro generation of exTregs resulted in a reduced number of DEGs in comparison with in vivo exTregs, in vitro–generated exTregs showed highly similar enrichment in Th17-associated genes (e.g., *Il17*, *Rorc*, and *Tnfsf11*) and reduced expression of Treg-associated genes (e.g., *Foxp3* and *Ctla4*) (Figure 9, A and B). When we compared the expression of 30 genes that have been reported to define the Th17 and Treg transcriptional programs (15, 33–36), we found very high similarity between exTregs isolated from fate-mapping mice and in vitro–generated exTregs (Figure 9C and Supplemental Figure 7,
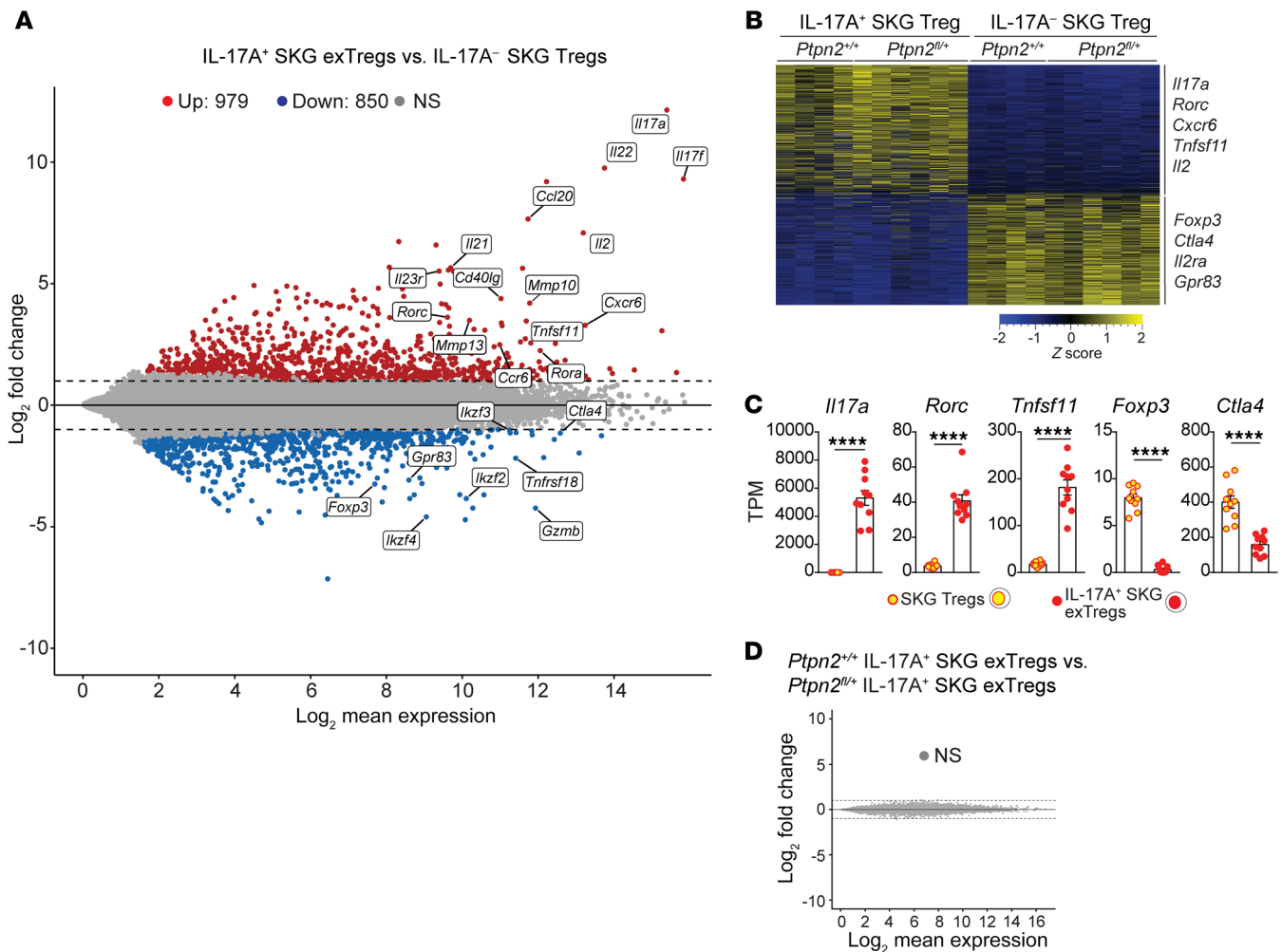
Figure 8. Transcriptomic comparison of in vivo isolated exTregs and Tregs. (**A–D**) RNA-Seq performed on IL-17A+ SKG exTregs and IL-17– SKG Tregs sorted from *Ptpn2fl/+* (*n* = 6) or *Ptpn2+/+* (*n* = 4) arthritic fate-mapping mice. (**A**) Mean-difference plot of significantly (fold change > 2 and adjusted *P* value < 0.05) upregulated (red) and downregulated (blue) genes in IL-17A+ exTregs versus IL-17A– Tregs. Gray represents nonsignificantly (NS) expressed genes. (**B**) Heatmap of transcripts per million (TPM) values generated using genes with a fold change greater than 2 and adjusted *P* value of less than 0.05. (**C**) Normalized expression of selected genes in SKG IL-17A+ exTregs and IL-17A– SKG Tregs. (**D**) MD plot comparing *Ptpn2+/+* and *Ptpn2+/–* IL-17A+ exTregs. Compiled data from at least 3 independent experiments are presented. Each symbol in **C** represents an individual mouse. Bars represent mean ± SEM. ****P* < 0.0001 by unpaired *t* test (**C**).

C and D). The similarity in gene expression profile between in vitro and in vivo exTregs was further supported by pathway analysis, which showed almost identical pathway enrichment between the 2 populations (Supplemental Figure 7E). Furthermore, as seen in vivo, there was no difference in gene expression profiles between in vitro–generated *Ptpn2+/+* and *Ptpn2+/–* exTregs (Supplemental Figure 7F). We conclude that in vitro IL-6–induced exTregs do display high phenotypic similarity to exTregs found in vivo in arthritic SKG mice. The residual difference between the transcriptomes of in vitro IL-6–induced and in vivo exTregs suggests that additional stimuli are needed to fully recapitulate in vitro either the population heterogeneity or the transcriptional program of in vivo exTregs.

exTregs display a unique chromatin landscape. Next, we assessed whether the generation of exTregs was also associated with changes in chromatin accessibility. SKG Tregs were stimulated with IL-6 in vitro and isolated after 24 hours (Tregs 24h), 48 hours (Tregs 48h), and 72 hours (Tregs 72h) of culture, and their chromatin accessi-

bility profiles were compared with those of exTregs isolated after 72 hours of stimulation (exTregs 72h) by assay for transposable-accessible chromatin with high-throughput sequencing (ATAC-Seq) (Figure 10A and Supplemental Figure 7G). Comparison of exTregs 72h with Tregs 24h identified more than 30,000 differentially accessible regions (Figure 10B), while comparison with Tregs 48h identified over 21,000 differentially accessible regions, and comparison with Tregs 72h showed around 15,000 differentially accessible regions (Figure 10, C and D). Furthermore, comparison of differentially accessible regions between Tregs at different stages of dedifferentiation demonstrated that exTregs possess a unique set of regions with enhanced or suppressed accessibility, while Tregs 48h displayed an expanded set of regions with enhanced accessibility when compared with Tregs at other time points (Figure 10, E–G).

Compared with Tregs, exTregs showed an almost complete lack of accessible chromatin pattern at the *Foxp3* loci, which was similar to that seen in sorted Th17 cells (Figure 10H). Evaluation
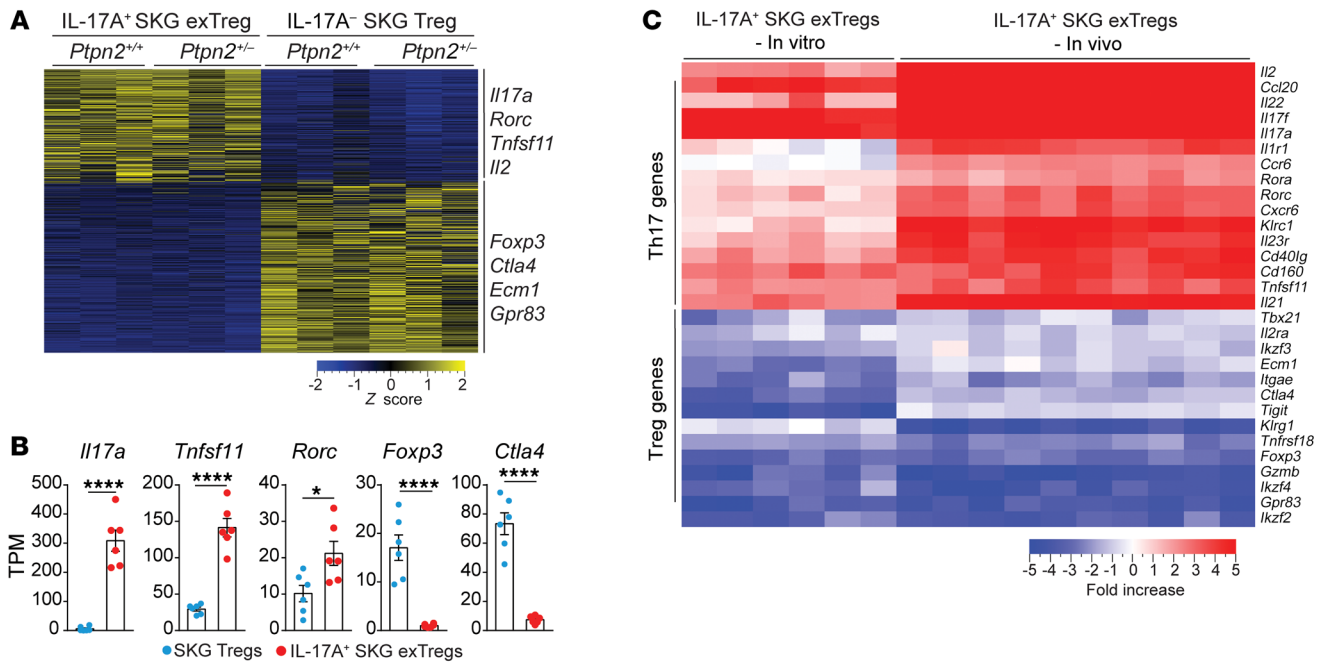
Figure 9. In vitro–generated exTregs recapitulate in vivo exTregs. (A–C) RNA-Seq analysis performed on IL-17+ SKG exTregs and IL-17− SKG Tregs generated in vitro from *Ptpn2*+/+ (n = 3) and *Ptpn2*+/− (n = 3) Tregs isolated from FoxP3eGFP SKG mice and stimulated for 72 hours with IL-6 (50 ng/ml) and anti-CD3/CD28–coated beads. **(B)** Normalized expression of selected genes in IL-17A+ SKG exTregs and IL-17A− SKG Tregs. **(C)** Expression of 30 genes associated with the transcriptional profile of Tregs and Th17 cells in in vitro IL-17A+ SKG exTregs and in vivo IL-17A+ SKG exTregs. Heatmap represents fold change between Tregs and exTregs generated from raw counts. Compiled data from 3 independent experiments are presented. Each symbol in **B** represents an individual mouse. Bars represent mean ± SEM. *$P < 0.05$, ****$P < 0.0001$ by unpaired *t* test (**B**).

of the *Rorc* loci showed gradually increasing chromatin accessibility during Treg dedifferentiation, and Tregs and exTregs after 72 hours displayed a pattern similar to that seen in Th17 cells (Figure 10I). However, in contrast to the *Rorc* loci, only exTregs showed a pattern of increased chromatin accessibility similar to that seen in Th17 cells in the extended *Il17a* and *Il17f* loci (Figure 10J).

Together these results suggest that during IL-6–driven dedifferentiation, Tregs undergo specific changes in chromatin accessibility that include a progressive opening of the *Rorc* loci. On the other hand, exTregs display a unique chromatin landscape compared with Tregs at other stages, characterized, among other changes, by the closure of the *Foxp3* loci and increased chromatin accessibility of the *Il17* loci, conducive to active *Il17* transcription. Furthermore, the concentration of newly opened loci at 48 hours of stimulation suggests that key molecular mechanisms of Treg destabilization occur at this stage.

Ptpn2 regulates stability of RORγt+ effector Tregs. Consistent with the above-mentioned chromatin accessibility assessment, analysis of in vitro SKG exTreg generation showed that IL-6–driven conversion into FoxP3− exTregs occurs via upregulation of RORγt in Tregs followed by subsequent loss of FoxP3 from RORγt+ Tregs and expression of IL-17 in RORγt+FoxP3− exTregs (Figure 11A). RORγt+ Tregs have been described in vivo as having an effector phenotype (37, 38). In line with previous reports, RORγt+ SKG Tregs displayed an effector phenotype with high expression of CD44 and low expression of CD62L and also showed high expression of ICOS and CCR6 similar to that seen in Th17 cells (Supplemental Figure 8A).

Next, we sorted effector and resting Tregs from *Ptpn2*+/+ and *Ptpn2*+/− FoxP3eGFP SKG mice and subjected them to in vitro conversion (Supplemental Figure 8B). We further confirmed that *Rorc* was primarily expressed in effector Tregs by quantitative PCR and flow cytometry (Supplemental Figure 8, B–D; expression of *Prdm1* was used to confirm sorting of effector Tregs). There was no difference in expression of *Foxp3* between sorted effector and resting Tregs (Supplemental Figure 8C); however, effector Tregs showed enhanced tendency to lose FoxP3 and convert into IL-17+ exTregs despite lower expression of IL-6 receptors (Figure 11, B–D, and Supplemental Figure 8E). As shown in Figure 11, B–D, *Ptpn2* haploinsufficiency (which resulted in 50% reduction of *Ptpn2* expression; Supplemental Figure 8F) selectively enhanced the in vitro conversion of effector but not resting Tregs into exTregs. This was not associated with decreased expression of CD25 in effector Tregs — which reportedly correlates with enhanced Treg to exTreg conversion (33) — or with differences in expression of RORγt between *Ptpn2*+/+ and *Ptpn2*+/− resting or effector Tregs (Supplemental Figure 8, A, G, and H). These data suggest that IL-17–producing exTregs are generated via loss of FoxP3 by effector RORγt+ Tregs and that *Ptpn2* selectively promotes FoxP3 stability in effector RORγt+ Tregs but not IL-6–induced expression of RORγt in Tregs.

Ptpn2 haploinsufficiency promotes IL-6–induced FoxP3 instability in effector RORγt+ Tregs. To further evaluate the mechanism by which IL-6 promotes conversion of Tregs into exTregs, we treated *Ptpn2*+/+ and *Ptpn2*+/− resting Tregs, which have low expression or no expression of RORγt, with ruxolitinib, an inhibitor of the JAK1–2/STAT3 pathway downstream of the IL-6 receptor (39, 40).
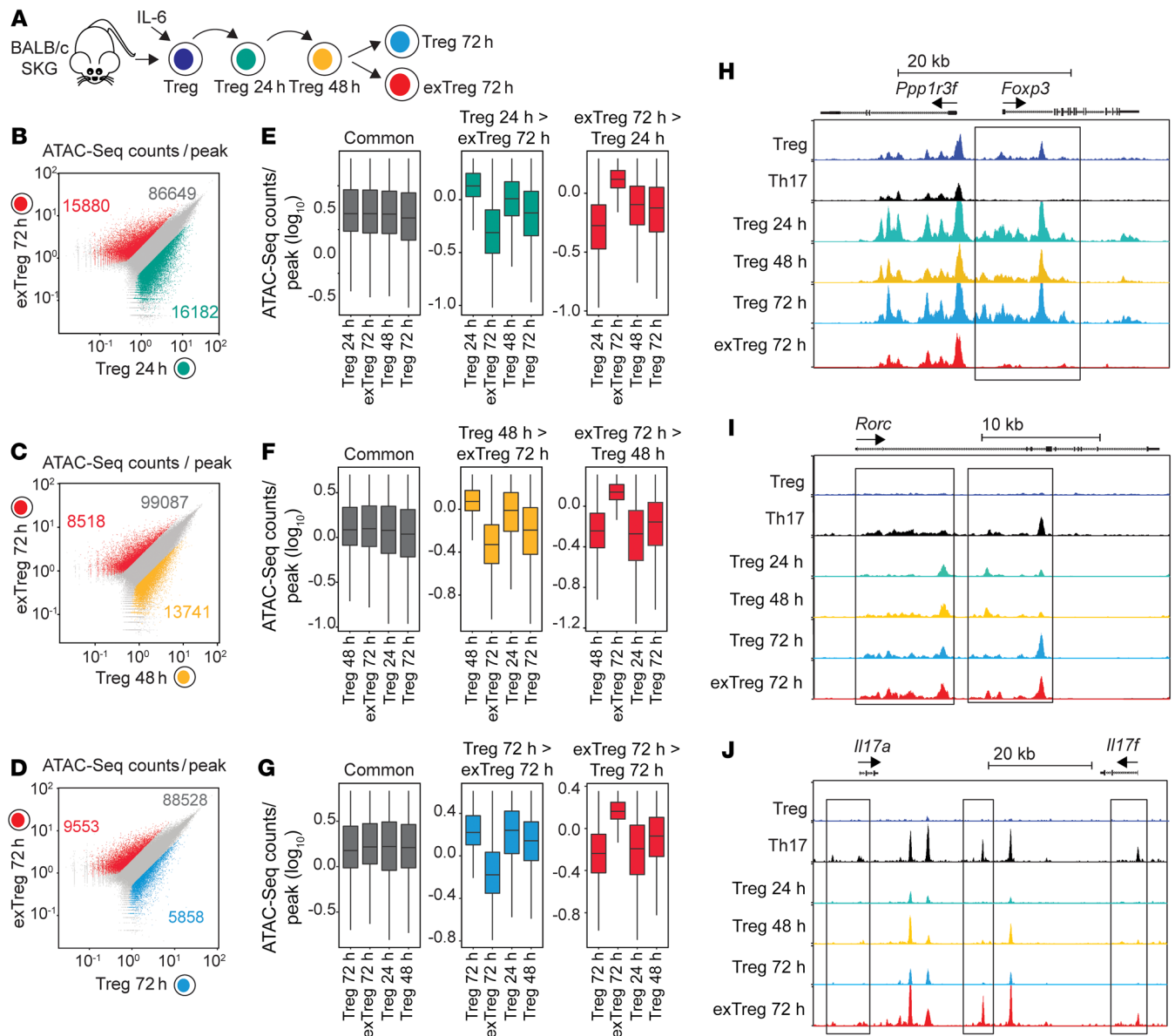
Figure 10. exTregs display a unique chromatin landscape. (**A**–**J**) ATAC-Seq for chromatin accessibility in SKG Tregs and SKG Th17 cells, as well as SKG Tregs during in vitro conversion and SKG exTregs. (**A**) Experimental design for evaluation of chromatin profile in SKG Tregs during in vitro conversion in the presence of IL-6 (50 ng/ml) and anti-CD3/CD28–coated beads. Tregs were isolated after 24, 48, and 72 hours of culture, whereas exTregs were isolated after 72 hours. (**B**–**D**) Scatterplots of ATAC-Seq counts per peak comparing indicated samples. (**E**–**G**) Boxplots of ATAC-Seq counts per peak from indicated samples at common or differentially accessible regions from the comparison labeled above. Boxes indicate interquartile range with whiskers ± 1.5 times this range and outlier points. (**H**–**J**) Normalized ATAC-Seq coverage at the *Foxp3* (**H**), *Rorc* (**I**), and *Il17a* and *Il17f* (**J**) loci in Tregs, Th17 cells, Tregs during in vitro conversion, and exTregs. Scale: 0–1200 for *Foxp3* and *Rorc*, 0–800 for *Il17a* and *Il17f*. Black rectangles represent visually evident changes in ATAC signal. ATAC-Seq from 2 independent replicates.

Ruxolitinib significantly reduced IL-6–induced loss of FoxP3 from RORγt⁺ Tregs and the generation of IL-17⁺ exTregs and obliterated the effect of *Ptpn2* haploinsufficiency on the conversion of RORγt⁺ Tregs into IL-17⁺ exTregs without affecting Treg survival within the time frame of the assay (Figure 11, E and F, and Supplemental Figure 8I). However, neither ruxolitinib nor *Ptpn2* haploinsufficiency affected IL-6–induced upregulation of RORγt in resting Tregs (Figure 11, E and F). These data provide evidence that Treg to exTreg conversion is promoted by IL-6–induced activation of the JAK/STAT pathway, although further studies in vivo — e.g.,

via ruxolitinib treatment — are warranted to solidify the role of this pathway for in vivo exTreg generation. Interestingly, inhibition of RORγt function did not block IL-6–induced loss of FoxP3 by RORγt⁺ Tregs, despite suppressing expression of IL-17 from exTregs (Supplemental Figure 8, J and K).

PTPN2 regulates FoxP3 stability in effector Tregs through binding and dephosphorylation of STAT3. In order to identify potential molecular mechanisms of action of PTPN2, we interrogated the above-mentioned chromatin landscape data looking for transcription factor (TF) binding motifs that are differentially accessi-
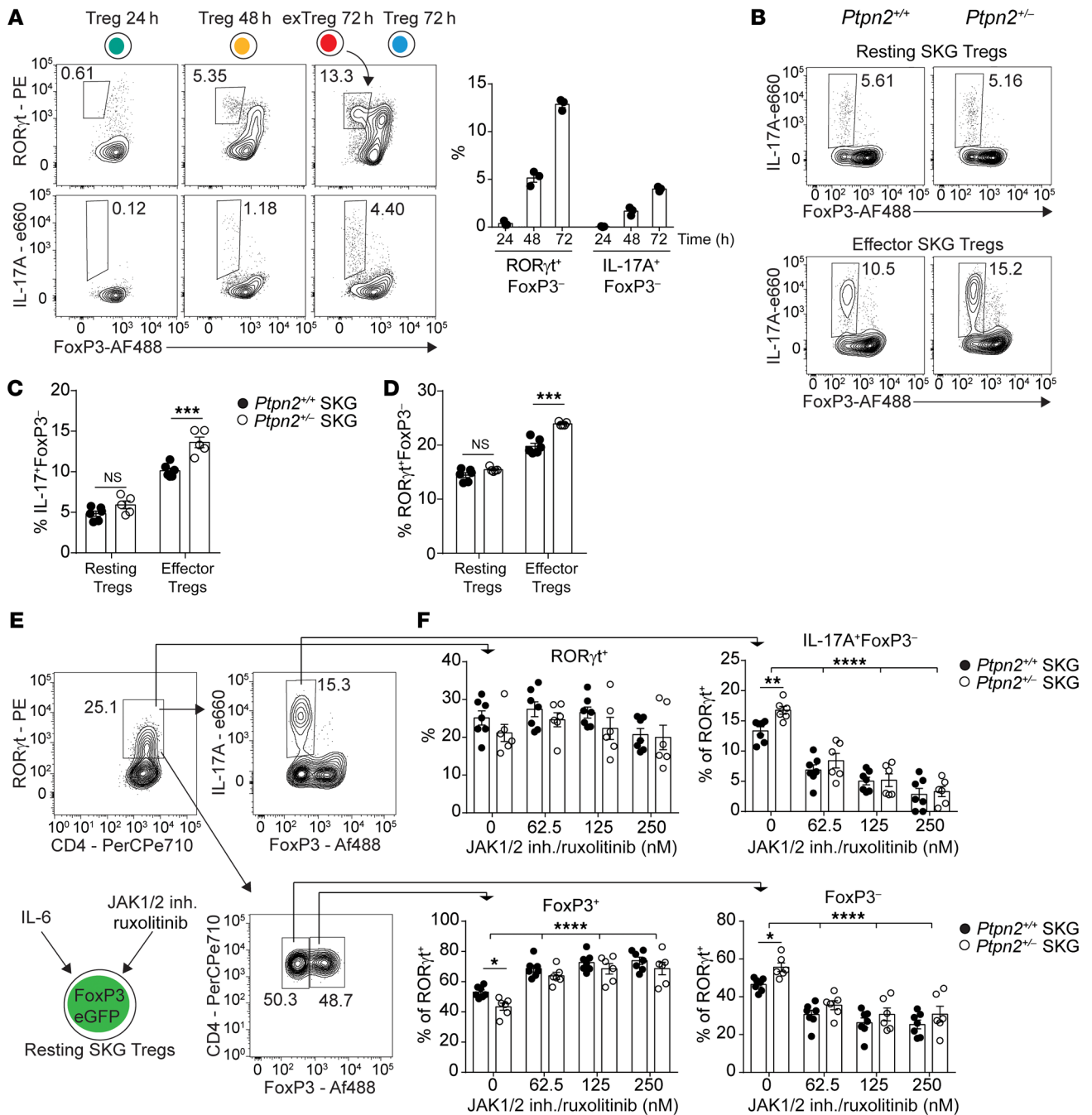
Figure 11. *Ptpn2* haploinsufficiency promotes conversion of RORγt⁺ effector Tregs. (A) Kinetics of IL-17A⁺ exTreg generation during in vitro stimulation of sorted *Ptpn2*⁺/⁺ FoxP3^eGFP SKG Tregs (*n* = 3) with IL-6 (50 ng/ml) and anti-CD3/CD28–coated beads. **(B and C)** In vitro conversion of *Ptpn2*⁺/⁺ (*n* = 6) and *Ptpn2*⁺/⁻ (*n* = 5) effector and resting SKG Tregs into IL-17⁺ exTregs. **(D)** Generation of FoxP3⁻RORγt⁺ exTregs (gated as in **A**) from *Ptpn2*⁺/⁺ and *Ptpn2*⁺/⁻ effector and resting SKG Tregs. **(E and F)** Inhibition of JAK1/2 signaling using ruxolitinib during in vitro conversion of resting SKG Tregs. **(E)** Gating strategy for evaluation of RORγt⁺ expressing *Ptpn2*⁺/⁺ (*n* = 7) and *Ptpn2*⁺/⁻ (*n* = 6) cells after 72 hours of culture. **(F)** Effect of JAK1/2 inhibition on upregulation of RORγt⁺ on live cells (top left, dot plot), generation of IL-17⁺FoxP3⁻ exTregs (top right, dot plot and histograms), and loss of FoxP3 within the RORγt⁺ population (bottom dot plot and histograms). Compiled data from 2 experiments are presented (**C–F**). Each symbol represents an individual mouse. Bars represent mean ± SEM. *$P < 0.05$, **$P < 0.01$, ***$P < 0.001$, ****$P < 0.0001$ by unpaired *t* test (**C and D**) or 2-way ANOVA (**F**).

ble at consecutive stages of IL-6–induced Treg dedifferentiation. We found that in the first 48 hours there was an enrichment of motifs for TFs belonging to the bZIP family, whereas accessibility of binding motifs for the ETS-family TFs was reduced. After an additional 24 hours the same trend toward increased accessibility for bZIP-family TFs and decreased accessibility for ETS-family TFs was observed in converted exTregs 72h, which in addition also displayed enrichment of motifs for Runt-family TFs. On the contrary, nonconverted Tregs 72h displayed an opposite profile characterized by enrichment of ETS-family TF motifs and
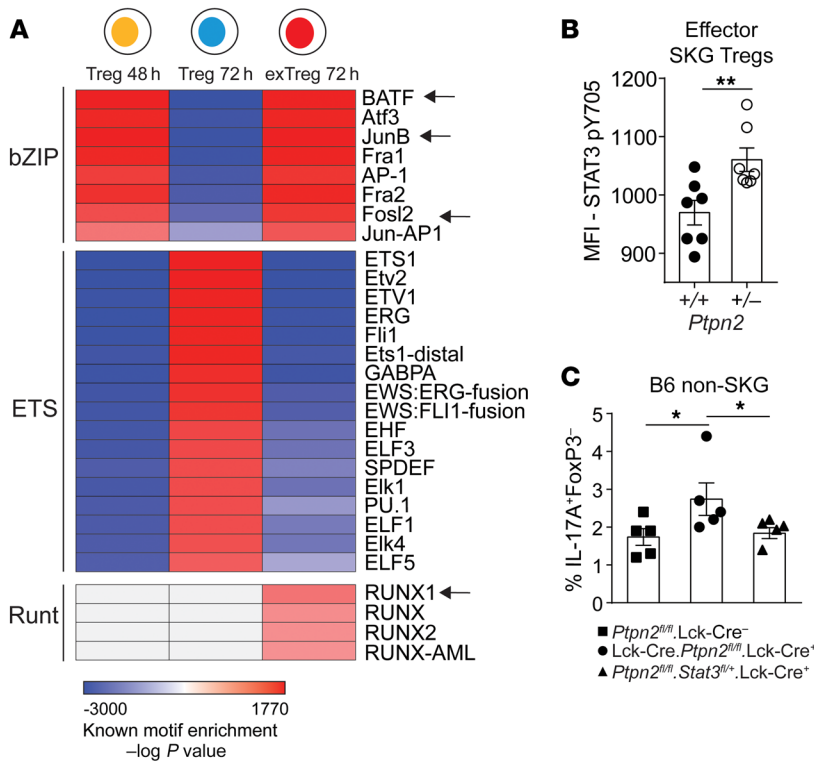
Figure 12. Increased conversion of *Ptpn2*-haploinsufficient Tregs is mediated through STAT3. (A) Motif enrichment analysis on differentially accessible regions identified by pairwise comparison of Tregs 24h versus Tregs 48h ("Treg 48 h"), Tregs 48h versus Tregs 72h ("Treg 72 h"), and Tregs 72h versus exTregs 72h ("exTreg 72 h"). Arrows indicate transcription factors that have been reported to associate with STAT3 functions in CD4^{+} T cells. Motifs with an enrichment log *P* value less than −35 and found in 10% or more regions and a fold increase of 2.5 over background were used to generate the heatmap. Motif enrichment analysis performed on ATAC-Seq experiment in Figure 10. **(B)** Activation of STAT3 (pY705) induced by 5 ng/ml IL-6 in *Ptpn2*^{+/+} and *Ptpn2*^{+/−} effector SKG Tregs, analyzed by flow cytometry. **(C)** In vitro conversion of *Ptpn2*^{fl/fl}.Lck-Cre[−] (*n* = 5), *Ptpn2*^{fl/fl}.Lck-Cre[+] (*n* = 5), and *Ptpn2*^{fl/fl}*Stat3*^{fl/+}.Lck-Cre[+] (*n* = 5) Tregs isolated from non-SKG B6 mice. Compiled data from 2 experiments are presented (**B** and **C**). Each symbol represents an individual mouse in **B** and **C**. Two independent replicates are used for ATAC-Seq heatmap. Bars represent mean ± SEM. **P* < 0.05, ***P* < 0.01 by unpaired *t* test (**B**) or Mann-Whitney (**C**).

reduction in bZIP-family TF motifs (Figure 12A). Several members of the bZIP transcription factor family (such as BATF, JunB, and Fosl2) have been associated with the Th17 differentiation program (35, 41), whereas members of the ETS family (such as ETS-1) have been associated with stabilization and functions of Tregs (42, 43). Among members of the Runt TF family, Runx1 has an important role in promoting IL-17 production through direct interaction with RORγt (44).

At no stage of Treg dedifferentiation could we observe differences in chromatin accessibility between *Ptpn2*^{+/+} and *Ptpn2*^{+/−} (Supplemental Figure 8L), suggesting that PTPN2 does not affect Treg dedifferentiation by skewing chromatin accessibility to the above-mentioned TFs. However, although we did not find enrichment of STAT3 binding motifs (but we cannot rule out effects before the time points considered in this study), we noticed that several TFs (indicated by arrows in Figure 12A) that bind to motifs displaying enhanced accessibility in Tregs 48h (the stage at which the conversion process is maximized) and in exTregs 72h are known in CD4^{+} T cells to mediate functions of STAT3 (35, 45).

Since STAT3 is a known substrate for PTPN2, we hypothesized that *Ptpn2* haploinsufficiency promotes Treg instability via abnormal regulation of STAT3 phosphorylation in RORγt[+] effector Tregs. Consistent with our hypothesis, we observed an enhanced activation of STAT3 in effector *Ptpn2*^{+/−} SKG Tregs after IL-6 stimulation when compared with *Ptpn2*^{+/+} SKG Tregs (Figure 12B). To confirm that PTPN2 regulates Treg conversion through an action on STAT3, we sorted Tregs from *Ptpn2*^{fl/fl} (PTPN2-WT), Lck-Cre.*Ptpn2*^{fl/fl} (PTPN2-KO), and Lck-Cre.*Ptpn2*^{fl/fl}.*Stat3*^{fl/+} (PTPN2-KO STAT3-het) B6 mice. PTPN2-KO Tregs showed enhanced susceptibility to conversion into exTregs, which was abrogated by semi-loss of STAT3 (Figure 12C and Supplemental Figure 8M).

In further support that STAT3 is a target for PTPN2 in Tregs, we could coimmunoprecipitate PTPN2 and STAT3 from lysates of in vitro–expanded Tregs (Figure 13A). To confirm a direct functional interaction between PTPN2 and STAT3, we performed in vitro dephosphorylation and substrate trapping experiments. In support of a direct role of PTPN2 in regulation of STAT3 activation, we found that PTPN2 dephosphorylates STAT3 pY705 (Figure 13B). Furthermore, we found that a substrate trapping mutant of PTPN2 (D182A, Q260A) could form a physical complex with phosphorylated STAT3 (pTyr705) but not with unphosphorylated STAT3 (Figure 13C).

Together, these results suggest a model (Figure 13D) where PTPN2 selectively inhibits JAK/STAT–dependent loss of FoxP3 in IL-6–stimulated RORγt[+] effector Tregs — at a stage when chromatin accessibility for Tregs destabilizing TFs is maximized — which in turn inhibits RORγt-dependent IL-17 production. IL-6–induced upregulation of RORγt in Tregs does not promote loss of FoxP3 and, surprisingly, appears to occur through a JAK- and PTPN2-independent pathway.

Discussion

In this study we aimed to clarify the functional genetics of *PTPN2* in autoimmunity by focusing on mouse models of RA carrying semideletion of *Ptpn2*, which reduces the expression of *Ptpn2* in immune cells to a level comparable to what has been reported in human carriers of *PTPN2* haplotypes associated with RA and inflammatory bowel disease. Global deletion of *Ptpn2* in BALB/c mice results in spontaneous subchondral bone erosion and synovitis; however, no further experimental investigation of the role of PTPN2 in RA has been reported (46). Although *Ptpn2* haploinsufficiency does not trigger spontaneous autoimmunity in B6 mice
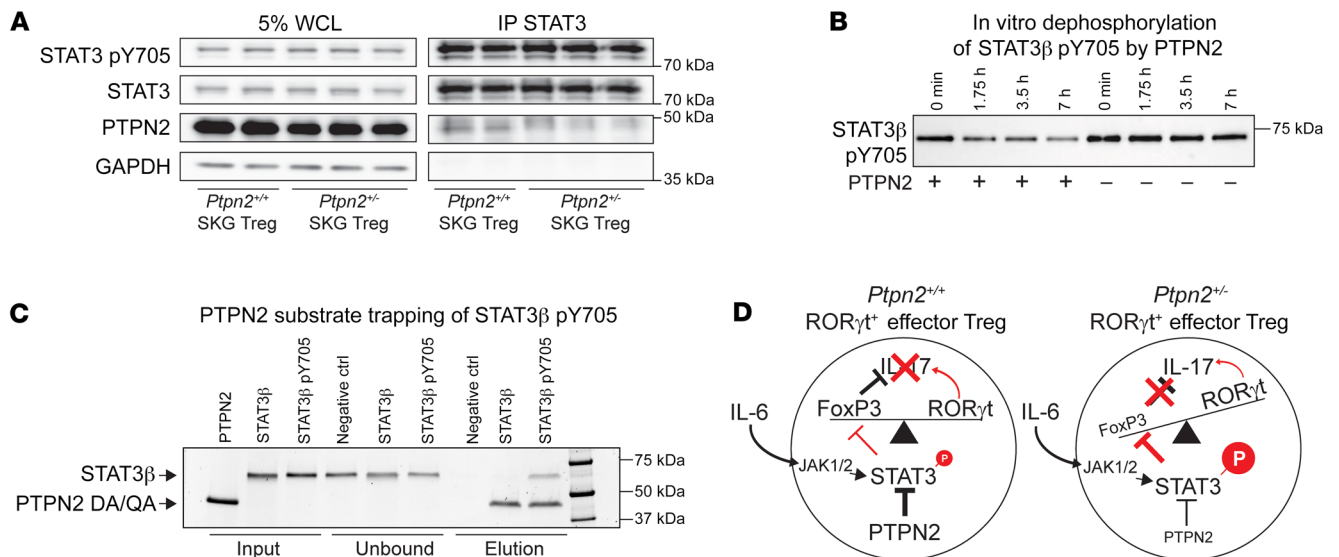
Figure 13. PTPN2 directly interacts with and dephosphorylates STAT3. (**A**) Immunoprecipitation of STAT3 in in vitro–expanded Tregs (expanded with IL-2 and anti-CD3/CD28–coated beads) after stimulation with IL-6 (50 ng/ml) for 20 minutes. All samples shown were separated on the same gel. WCL, whole cell lysate. (**B**) Dephosphorylation of STAT3β pY705 after incubation with (+) or without (–) recombinant PTPN2. Samples were taken at 0, 1 hour 45 minutes, 3 hours 30 minutes, and 7 hours for analysis. All samples shown were separated on the same gel. (**C**) Substrate trapping of STAT3β pY705 by the PTPN2 mutant (D182A, Q260A). Unphosphorylated STAT3β was used as a negative control and does not bind PTPN2, as shown. Proteins were analyzed by SDS-PAGE and run on the same gel. (**D**) Schematic of proposed mechanism by which partial loss of function in PTPN2 in Tregs promotes STAT3-mediated loss of FoxP3 and generation of IL-17A–producing exTregs. Representative experiments out of 2 (**A**) and 3 (**B** and **C**) independent replicates are shown. See complete unedited blots in the supplemental material.

(9), we show that it is able to enhance incidence and severity of disease on an autoimmune-prone background. This exemplifies the importance of modeling human autoimmune-associated variants in an autoimmunity-prone context, reflecting the additional risk factors that are needed in humans to trigger disease.

Our data point to haploinsufficiency of *Ptpn2* being able to sustain some but not all of the immunological functions reported for *Ptpn2* (9–11, 29). For example, while complete deletion or deep knockdown of *Ptpn2* revealed a major role of this enzyme in limiting myeloid cell– and synoviocyte-driven inflammation (7, 18), we find that innate immune cells are not critical mediators of the pathogenic action of *Ptpn2* haploinsufficiency. We show here that *Ptpn2* haploinsufficiency in autoreactive T cells promotes expansion of Th1, Treg, and pathogenic Th17 cells under lymphopenic conditions. Complete deletion of *Ptpn2* is known to promote lymphopenic expansion of naive CD4+ and CD8+ T cells through enhancement of TCR signaling, while IL-7 signaling was unaffected (29). However, we did not find significant evidence of increased TCR signaling in *Ptpn2*-haploinsufficient SKG mice. Similarly, conditional haploinsufficiency of *Ptpn2* in T cells on the B6 background did not result in increased TCR sensitivity or altered thymic selection (9). On the other hand, the enhanced IL-2 signaling found in *Ptpn2*-haploinsufficient T cells is reminiscent of the phenotype of *Ptpn2−/−* T cells, which display increased IL-2–mediated Treg expansion (9, 47). Thus, we speculate that enhanced IL-2 signaling underlies the observed expansion of *Ptpn2*-haploinsufficient Th1 cells and Tregs in lymphopenic conditions. *Ptpn2* haploinsufficiency also led to marked expansion of pathogenic IL-17–producing CD4+ T cells after transfer of SKG CD4+ T cells into lymphopenic hosts. However, in contrast to previous reports on naive *Ptpn2−/−*

T cells, *Ptpn2*-haploinsufficient naive CD4+ T cells did not show increased IL-6–driven differentiation into Th17. This could be due to differences between WT and SKG naive T cells or between IL-6 and IL-2 signaling amplification in *Ptpn2−/−* versus *Ptpn2+/−* T cells.

Here we suggest that loss of FoxP3 by RORγt+ Tregs significantly contributes to the increased numbers of IL-17–producing cells observed in *Ptpn2+/−* arthritic mice. We show that Treg-specific haploinsufficiency of *Ptpn2* is sufficient to enhance severity of arthritis in SKG mice and replicates the phenotype seen in mice carrying haploinsufficiency of *Ptpn2* in all T cells. We did not find any defect of suppressive function of *Ptpn2*-haploinsufficient Tregs, consistent with previous data in mice carrying complete deletion of *Ptpn2* (9). However, *Ptpn2*-haploinsufficient RORγt+ Tregs are more sensitive to IL-6–dependent loss of FoxP3 and conversion into IL-17A–producing exTregs that can transfer arthritis to Rag2-KO recipient mice. Since no conditional deletion of *Ptpn2* or of other tyrosine phosphatases in Tregs has been reported to date and the role of *Ptpn2* in Tregs in the context of inflammation has not been explored yet, our results also highlight for the first time a potential role of a tyrosine phosphatase in Treg stability in the context of autoimmune inflammation.

Since it has been reported that complete loss of *Ptpn2* causes expansion of Tregs and enhances FoxP3 stability in inducible Tregs (9, 16), we were surprised to find that *Ptpn2* haploinsufficiency promotes autoimmunity through destabilization of Tregs. Also the enhanced in vitro IL-2 signaling observed in *Ptpn2*-haploinsufficient naive CD4+ T cells and the potentially IL-2 signaling–dependent expansion of disease-protective Th1 cells and Tregs in lymphopenic animals might sound inconsistent with the proposed arthritogenic role of *Ptpn2* haploinsufficiency in SKG mice. However, in arthritic *Ptpn2+/−* SKG mice we could not detect any expan-

sion of Th1 cells or Tregs. Thus, in nonlymphopenic conditions, the IL-2 signaling–enhancing effect of *Ptpn2* haploinsufficiency might be limited and/or its disease-protective effect neutralized by enhanced IL-6 signaling, which also might offset any potential Treg expansion via Treg destabilization.

Our data lend support to previous observations that loss of FoxP3 in Tregs is responsible for generation of pathogenic T cells during autoimmune diabetes (48) and in CIA (33). However, the molecular mechanism of FoxP3 loss in Tregs has remained unexplored. Here we show that during IL-6–driven dedifferentiation, Tregs undergo specific changes in chromatin accessibility. In this context, enhanced IL-6–dependent loss of FoxP3 in *Ptpn2*-haploinsufficient Tregs correlates with enhanced phosphorylation of STAT3, and depends on JAK activity and STAT3 expression. Importantly, T cell phenotyping and chromatin analysis shows that loss of *Ptpn2* selectively destabilizes effector Tregs and suggests that STAT3 phosphorylation in Tregs is only able to modulate FoxP3 stability in RORγt+ Tregs, without affecting IL-6–dependent RORγt expression. Thus, our data also suggest potential differences in signaling pathways mediating IL-6–dependent RORγt induction and in downstream STAT3-dependent signaling between Tregs and FoxP3− T cells.

In conclusion, reduced *Ptpn2* expression promotes arthritis through enhanced IL-6 signaling in effector Tregs, causing increased STAT3 phosphorylation that renders RORγt+ Tregs more susceptible to loss of FoxP3. It remains to be established whether the arthritogenic effect of *Ptpn2* haploinsufficiency is exerted on natural Tregs and/or peripherally induced Tregs. Also, the importance of PTPN2 as a regulator of JAK/STAT signaling suggests that further studies are warranted on the potential role of *Ptpn2* haploinsufficiency in enhancing signaling of additional JAK/STAT activator cytokines that might play a role in the pathogenesis of SKG arthritis (e.g., IL-23 and IL-10).

Our study shows the importance of considering gene dosage when performing functional genetics studies and sheds light on unexpected functions of tyrosine phosphatases and the potential uniqueness of signaling pathways involved in Treg stability. Further studies of tyrosine phosphatases in resting versus effector Tregs and of the molecular program underlying STAT3-dependent loss of FoxP3 in effector Tregs hold the promise of unraveling novel mechanisms of tolerance and autoimmunity.

Methods

Mice. SKG mice have already been described (23). *Ptpn2*+/− BALB/c mice have been previously described (12). Generation of *Ptpn2*-floxed (*Ptpn2fl/fl*) B6 mice has recently been described (49). B6 mice congenic for the H2d haplotype (JAX 000359, B6.C-*H2d*/bByJ), and B6 FoxP3YFP-Cre [JAX 016959, B6.129(Cg)-*Foxp3tm4(YFP/iCre)Ayr*/J; ref. 50], B6 ROSA-26-tdTomato [JAX 007914, B6;Cg-*Gt(ROSA)26Sortm14(CAG-tdTomato)Hze*/J; ref. 51], BALB/c FoxP3-eGFP (JAX 006769, C.Cg-*Foxp3tm2Tch*/J; ref. 52), BALB/c CD45.1 [JAX 006584, CByJ.SJL(B6)-*Ptprca*/J], and BALB/c (JAX 000651, BALB/cJ) mice, were all obtained from The Jackson Laboratory. BALB/c Rag2-KO mice were purchased from Taconic (model 601). The above mice were housed at the La Jolla Institute for Allergy and Immunology (LJI) and UCSD vivarium under specific pathogen–free conditions. *Ptpn2fl/fl*. Lck-Cre+ (B6) (9) and *Stat3floxed* mice were housed at the Peter MacCallum Cancer Centre (Melbourne, Australia).

Arthritis models. For the K/BxN serum transfer model, arthritis was induced in 8-week-old male BALB/c mice by i.p. injection of serum obtained from arthritic K/BxN mice. Every 2 days, development of arthritis was assessed by measurement of ankle thickness using a digital caliper according to an established protocol (53).

For the SKG mouse model, both spontaneous and mannan-induced arthritis were assessed. For mannan-induced arthritis, male and female mice were injected i.p. with 20 mg of mannan (Sigma-Aldrich), dissolved in sterile PBS at 8 weeks of age. Clinical scoring and measurement of ankle thickness using a digital caliper was performed twice weekly according to an established protocol (24). Briefly, clinical signs of arthritis in front and hind paws were scored as follows: 0, no joint swelling; 0.1 per swollen finger joint (3 digits on front paw and 4 digits on hind paw); 0.5, mild swelling of wrist or ankle; 1.0, severe swelling of wrist or ankle. Scores for all finger joints of forepaws and hind paws, wrists, and ankles were combined for each mouse, yielding a maximum score of 5.4, which was considered the clinical endpoint. Mice reaching clinical endpoint scores were sacrificed according to ethical guidelines.

For neutralization of IL-17, female and male SKG mice or Rag2-KO mice were injected with 100 μg of anti–IL-17 antibody (clone 17F3, Bio X Cell) both retro-orbitally and i.p. 1–2 hours before injection of mannan, after which mice received anti–IL-17 antibody once weekly (100 μg) by i.p. injection. For neutralization of IL-6 signaling, male SKG mice received weekly i.p. injections of 200 μg anti–IL-6R (clone 15A7, Bio X Cell) antibody, with the first injection performed 2 hours before injection of mannan. Antibody-treated mice were compared with control untreated mice.

All arthritis studies were performed on littermate mice. For treatment experiments, mice with the same genotype were randomly selected for treatment with cytokine-neutralizing or control. Clinical scoring of mice was performed in a blinded manner in which genotypes and treatments were unknown to the researcher during scoring.

CD4+ T cell transfer and generation of T cell chimeras in Rag2-KO mice. CD4+ T cells (2 × 10⁶) isolated from spleen and lymph nodes of 8-week-old male *Ptpn2*+/+ and *Ptpn2*+/− SKG mice using the EasySep Mouse CD4 T Cell Enrichment Kit (Stem Cell Technologies) were transferred to 8-week-old male Rag2-KO BALB/c mice through retro-orbital injection. The purity of isolated cells was verified by flow cytometry and was typically 95%–98% with no contaminating B cells or CD8+ T cells. Spontaneous development of arthritis was evaluated by clinical scoring and ankle thickness as described above.

For CD4+ T cell chimera experiments, CD4+ T cells were isolated from spleen and lymph nodes of 8-week-old male CD45.1 and CD45.2 *Ptpn2*+/+ and *Ptpn2*+/− SKG using the EasySep Mouse CD4 T Cell Enrichment Kit (Stem Cell Technologies). CD4+ T cells (1 × 10⁶) from CD45.1 and CD45.2 mice were pooled in a 1:1 ratio (total of 2 × 10⁶ CD4+ T cells per mouse) and transferred into 8-week-old male Rag2-KO mice. To account for any differences between CD45.1 and CD45.2 SKG mice, *Ptpn2*+/+ and *Ptpn2*+/− CD4+ T cells were isolated from both CD45.1 and CD45.2 mice and cotransferred with the opposite genotype isolated from either CD45.1 or CD45.2 mice.

In vitro Treg conversion assay. In vitro conversion assay of FoxP3+ Tregs was performed using a protocol adopted from Komatsu et al. (33). Total FoxP3eGFP+ SKG Tregs (Supplemental Figure 5I) or effector (CD44hiCD62L−) and resting (CD44loCD62L+) FoxP3eGFP+ Tregs (Supplemental Figure 8B) were flow-sorted from *Ptpn2*+/+ and *Ptpn2*+/− 8- to 10-week-old female FoxP3eGFP+ SKG mice. Sorted Tregs were stimu-

lated with Dynabeads mouse anti-CD3/CD28 T cell activation beads (Invitrogen) with or without addition of IL-6 (BioLegend; 50 ng/ml) for 24–72 hours. At the end of stimulation, cells were restimulated with PMA (20 ng/ml), ionomycin (1 μM), and brefeldin A for 5 hours and analyzed for the expression of IL-17A, FoxP3, and RORγt using flow cytometry. Ruxolitinib (Selleck Chemical) was used for inhibition of JAK1/2 signaling, and the inverse agonist GSK805 (EMD Millipore Calbiochem) was used for inhibition of RORγt function.

For conversion assay using *Ptpn2*$^{fl/fl}$.Lck-Cre$^-$ and *Ptpn2*$^{fl/fl}$*Stat3*$^{fl/+}$. Lck-Cre$^+$ (PTPN2-KO STAT3-het) B6 mice, CD4$^+$CD25$^+$ Tregs were sorted by flow cytometry and stimulated with plate-bound anti-CD3 (10 μg/ml) and soluble anti-CD28 (5 μg/ml) for 72 hours in the presence of IL-6 (50 ng/ml). After 72 hours, cells were stimulated in the presence of ionomycin (1 μg/ml), PMA (20 ng/ml), and BD Golgi-Plug (BD Biosciences) and analyzed for the expression of IL-17A, RORγt, and FoxP3 using flow cytometry.

Further information regarding antibodies used for flow cytometry staining can be found in Supplemental Methods.

In vivo Treg stability assay and transfer of exTregs to Rag2-KO mice. Tregs (CD4$^+$FoxP3^{eGFP+}) were flow-sorted from spleen and lymph nodes of 8-week-old female *Ptpn2*$^{+/+}$ or *Ptpn2*$^{+/-}$ CD45.2 FoxP3^{eGFP} SKG mice, whereas CD4$^+$CD25$^-$ cells were sorted from 8-week-old female *Ptpn2*$^{+/+}$ or *Ptpn2*$^{+/-}$ CD45.1 SKG mice (Supplemental Figure 5, I and J). CD45.2 Tregs (3 × 10^5) were transferred in combination with CD45.1 CD4$^+$CD25$^-$ SKG T cells (1.3 × 10^6) to 8-week-old female Rag2-KO mice. One week after transfer, mice were injected with 20 mg of mannan to boost induction of arthritis. Tregs were analyzed in lymph nodes of arthritic mice using flow cytometry.

For evaluation of the pathogenicity of exTregs, Tregs were sorted from female *Ptpn2*$^{+/+}$ or *Ptpn2*$^{+/-}$ CD45.2 FoxP3^{eGFP} SKG mice as above. Isolated Tregs were subjected to in vitro conversion as described above. After 72 hours, *Ptpn2*$^{+/+}$ or *Ptpn2*$^{+/-}$ FoxP3^{eGFP-} exTregs were sorted (Supplemental Figure 7G) and transferred to female Rag2-KO mice (1.5 × 10^5 cells per mouse). Arthritis was induced 4 days after transfer by an i.p. injection with 20 mg of mannan. Mice were monitored for development of arthritis as described above.

Isolation of IL-17$^+$ exTregs and Tregs for RNA sequencing. Isolation of in vivo IL-17$^+$ exTregs from B6.SKG.H2$^{d/d}$.FoxP3$^{YFP-Cre+/-}$.tdTom$^{fl/+}$. *Ptpn2*$^{fl/+}$ or $^{+/+}$ was achieved using a mouse IL-17 Secretion Assay kit (Miltenyi Biotec Inc., 130-094-207) according to the manufacturer's protocol. Briefly, a single-cell suspension was prepared from spleen and lymph nodes of female B6.SKG.H2$^{d/d}$.FoxP3$^{YFP-Cre+/-}$.tdTom$^{fl/+}$. *Ptpn2*$^{fl/+}$ or B6.SKG.H2$^{d/d}$.FoxP3$^{YFP-Cre+/-}$.tdTom$^{fl/+}$.*Ptpn2*$^{+/+}$ arthritic mice (50–70 days after mannan). Cells were stimulated with PMA (10 ng/ml) and ionomycin (1 μg/ml) in TexMACS media (Miltenyi Biotec) containing 5% mouse serum for 3 hours, after which cells were stained with a streptavidin-labeled IL-17 capture reagent and incubated for 45 minutes. Cells were counterstained with anti-biotin–APC, CD4, TCRβ, CD8, CD19, and fixable viability dye. IL-17$^+$ exTregs (live cells CD8$^-$CD19$^-$TCRβ$^+$CD4$^+$tdTom$^+$YFP$^-$IL-17A$^+$) and IL-17$^-$ Tregs (live cells CD8$^-$CD19$^-$TCRβ$^+$CD4$^+$tdTom$^+$YFP$^+$IL-17A$^-$) were flow-sorted directly into Trizol LS (Supplemental Figure 6C).

For isolation of in vitro–generated IL-17$^+$ exTregs, Tregs (CD8$^-$CD19$^-$CD4$^+$FoxP3^{eGFP+}) were sorted from female *Ptpn2*$^{+/+}$ or *Ptpn2*$^{+/-}$ FoxP3^{eGFP} SKG mice. Isolated Tregs were subjected to in vitro conversion as described above. IL-17$^+$ exTregs and IL-17$^-$ Tregs were isolated (Supplemental Figure 7A) using the IL-17 Secretion kit as described above.

Isolation of cells for ATAC sequencing. Th17 cells (live CD8$^-$CD19$^-$CD4$^+$FoxP3^{eGFP}CCR6^{hi}) and Tregs (live CD8$^-$CD19$^-$CD4$^+$FoxP3^{eGFP+}) were flow-sorted from *Ptpn2*$^{+/+}$ and *Ptpn2*$^{+/-}$ female FoxP3^{eGFP} SKG mice (Supplemental Figure 7G). Th17 cells and Tregs (1 × 10^5) were directly prepared for ATAC-Seq (described in Supplemental Methods). Remaining Tregs were subjected to in vitro conversion as described above. FoxP3^{eGFP+} (Treg) cells were flow-sorted after 24, 48, and 72 hours of culture. FoxP3^{eGFP-} (exTregs) were sorted after 72 hours of culture (Supplemental Figure 7G).

Additional information regarding experimental methods can be found in Supplemental Methods.

Statistics. Sample sizes were selected based on our experience with the above-mentioned assays in order to achieve sufficient power to detect biologically relevant differences in the experiments being conducted with an α error (2-tailed) less than 0.05.

For statistical analysis, 2-tailed Mann-Whitney *U* test was performed on nonparametric data. On normally distributed data, 2-tailed paired *t* test or 2-tailed unpaired *t* test was performed as reported in the figure legends. For comparison of multiple parameters, 2-way ANOVA was used. All statistical analyses were performed using GraphPad Prism software. A comparison was considered significant if *P* was less than 0.05.

Study approval. The studies in animals were conducted in accordance with protocols approved by the Institutional Animal Care and Use Committee (IACUC) of the LJI (protocol AP140-NB4) and the IACUC of UCSD (protocol S16098), and in accordance with the National Health and Medical Research Council Australian Code of Practice for the Care and Use of Animals under approval of the Peter MacCallum Animal Ethics and Experimentation Committee (Ethics number AEEC 570, 604).

Author contributions

MNDS and NB conceived of, designed, and supervised the research, analyzed data, and wrote the paper. MNDS, KMD, BJS, DJW, CS, WBK, BP, SB, FW, RG, GS, ES, and SY contributed to acquisition and analysis of data. IA, GK, PM, SS, MK, MLT, PV, TT, and FA provided tools and/or reagents and key scientific input. All authors approved the final version of the paper.

Acknowledgments

Address correspondence to: Nunzio Bottini, Department of Medicine, University of California, San Diego, ACTRI, 9452 Medical Center Drive, La Jolla, California 92037, USA. Phone: 858.246.2398; Email: nbottini@ucsd.edu.

1. McInnes IB, Schett G. The pathogenesis of rheumatoid arthritis. *N Engl J Med*. 2011;365(23):2205–2219.

2. Viatte S, Plant D, Raychaudhuri S. Genetics and epigenetics of rheumatoid arthritis. *Nat Rev Rheumatol*. 2013;9(3):141–153.

3. Wellcome Trust Case Control Consortium. Genome-wide association study of 14,000 cases of seven common diseases and 3,000 shared controls. *Nature*. 2007;447(7145):661–678.

4. Lees CW, Barrett JC, Parkes M, Satsangi J. New IBD genetics: common pathways with other diseases. *Gut*. 2011;60(12):1739–1753.

5. Long SA, et al. An autoimmune-associated variant in PTPN2 reveals an impairment of IL-2R signaling in CD4(+) T cells. *Genes Immun*. 2011;12(2):116–125.

6. Scharl M, et al. Crohn's disease-associated polymorphism within the PTPN2 gene affects muramyl-dipeptide-induced cytokine secretion and autophagy. *Inflamm Bowel Dis*. 2012;18(5):900–912.

7. Doody KM, Bourdeau A, Tremblay ML. T-cell protein tyrosine phosphatase is a key regulator in immune cell signaling: lessons from the knock-out mouse model and implications in human disease. *Immunol Rev*. 2009;228(1):325–341.

8. van Vliet C, et al. Selective regulation of tumor necrosis factor-induced Erk signaling by Src family kinases and the T cell protein tyrosine phosphatase. *Nat Immunol*. 2005;6(3):253–260.

9. Wiede F, et al. T cell protein tyrosine phosphatase attenuates T cell signaling to maintain tolerance in mice. *J Clin Invest*. 2011;121(12):4758–4774.

10. Wiede F, et al. PTPN2 regulates T cell lineage commitment and αβ versus γδ specification. *J Exp Med*. 2017;214(9):2733–2758.

11. Wiede F, Sacirbegovic F, Leong YA, Yu D, Tiganis T. PTPN2-deficiency exacerbates T follicular helper cell and B cell responses and promotes the development of autoimmunity. *J Autoimmun*. 2017;76:85–100.

12. You-Ten KE, et al. Impaired bone marrow microenvironment and immune function in T cell protein tyrosine phosphatase-deficient mice. *J Exp Med*. 1997;186(5):683–693.

13. Spalinger MR, et al. PTPN2 controls differentiation of CD4⁺ T cells and limits intestinal inflammation and intestinal dysbiosis. *Mucosal Immunol*. 2015;8(4):918–929.

14. Sakaguchi S, Yamaguchi T, Nomura T, Ono M. Regulatory T cells and immune tolerance. *Cell*. 2008;133(5):775–787.

15. Rudensky AY. Regulatory T cells and Foxp3. *Immunol Rev*. 2011;241(1):260–268.

16. Bothur E, et al. Antigen receptor-mediated depletion of FOXP3 in induced regulatory T-lymphocytes via PTPN2 and FOXO1. *Nat Commun*. 2015;6:8576.

17. Schmiedel BJ, et al. 17q21 asthma-risk variants switch CTCF binding and regulate IL-2 production by T cells. *Nat Commun*. 2016;7:13426.

18. Aradi B, et al. Protein tyrosine phosphatase nonreceptor type 2: an important regulator of interleukin-6 production in rheumatoid arthritis synovial fibroblasts. *Arthritis Rheumatol*.

2015;67(10):2624–2633.

19. Lee DM, et al. Cadherin-11 in synovial lining formation and pathology in arthritis. *Science*. 2007;315(5814):1006–1010.

20. Ji H, et al. Arthritis critically dependent on innate immune system players. *Immunity*. 2002;16(2):157–168.

21. Nandakumar KS, Svensson L, Holmdahl R. Collagen type II-specific monoclonal antibody-induced arthritis in mice: description of the disease and the influence of age, sex, and genes. *Am J Pathol*. 2003;163(5):1827–1837.

22. Kagari T, Doi H, Shimozato T. The importance of IL-1 beta and TNF-alpha, and the noninvolvement of IL-6, in the development of monoclonal antibody-induced arthritis. *J Immunol*. 2002;169(3):1459–1466.

23. Hashimoto M, et al. Complement drives Th17 cell differentiation and triggers autoimmune arthritis. *J Exp Med*. 2010;207(6):1135–1143.

24. Sakaguchi N, et al. Altered thymic T-cell selection due to a mutation of the ZAP-70 gene causes autoimmune arthritis in mice. *Nature*. 2003;426(6965):454–460.

25. Hata H, et al. Distinct contribution of IL-6, TNF-α, IL-1, and IL-10 to T cell-mediated spontaneous autoimmune arthritis in mice. *J Clin Invest*. 2004;114(4):582–588.

26. Pitzalis C, Kelly S, Humby F. New learnings on the pathophysiology of RA from synovial biopsies. *Curr Opin Rheumatol*. 2013;25(3):334–344.

27. Grogan JL, Ouyang W. A role for Th17 cells in the regulation of tertiary lymphoid follicles. *Eur J Immunol*. 2012;42(9):2255–2262.

28. Jones GW, et al. Interleukin-27 inhibits ectopic lymphoid-like structure development in early inflammatory arthritis. *J Exp Med*. 2015;212(11):1793–1802.

29. Wiede F, La Gruta NL, Tiganis T. PTPN2 attenuates T-cell lymphopenia-induced proliferation. *Nat Commun*. 2014;5:3073.

30. Liao W, Lin JX, Wang L, Li P, Leonard WJ. Modulation of cytokine receptors by IL-2 broadly regulates differentiation into helper T cell lineages. *Nat Immunol*. 2011;12(6):551–559.

31. Hirota K, et al. T cell self-reactivity forms a cytokine milieu for spontaneous development of IL-17⁺ Th cells that cause autoimmune arthritis. *J Exp Med*. 2007;204(1):41–47.

32. Bettelli E, et al. Reciprocal developmental pathways for the generation of pathogenic effector TH17 and regulatory T cells. *Nature*. 2006;441(7090):235–238.

33. Komatsu N, et al. Pathogenic conversion of Foxp3⁺ T cells into TH17 cells in autoimmune arthritis. *Nat Med*. 2014;20(1):62–68.

34. Korn T, Bettelli E, Oukka M, Kuchroo VK. IL-17 and Th17 Cells. *Annu Rev Immunol*. 2009;27:485–517.

35. Ciofani M, et al. A validated regulatory network for Th17 cell specification. *Cell*. 2012;151(2):289–303.

36. Sugimoto N, et al. Foxp3-dependent and -independent molecules specific for CD25⁺CD4⁺ natural regulatory T cells revealed by DNA microarray analysis. *Int Immunol*. 2006;18(8):1197–1209.

37. Ohnmacht C, et al. The microbiota regulates type 2 immunity through RORγt⁺ T cells. *Science*. 2015;349(6251):989–993.

38. Sefik E, et al. Individual intestinal symbionts induce a distinct population of RORγ⁺ regulatory T cells. *Science*. 2015;349(6251):993–997.

39. Quintás-Cardama A, et al. Preclinical characterization of the selective JAK1/2 inhibitor INCB018424: therapeutic implications for the treatment of myeloproliferative neoplasms. *Blood*. 2010;115(15):3109–3117.

40. Fridman JS, et al. Preclinical evaluation of local JAK1 and JAK2 inhibition in cutaneous inflammation. *J Invest Dermatol*. 2011;131(9):1838–1844.

41. Schraml BU, et al. The AP-1 transcription factor Batf controls T(H)17 differentiation. *Nature*. 2009;460(7253):405–409.

42. Mouly E, et al. The Ets-1 transcription factor controls the development and function of natural regulatory T cells. *J Exp Med*. 2010;207(10):2113–2125.

43. Rudra D, et al. Transcription factor Foxp3 and its protein partners form a complex regulatory network. *Nat Immunol*. 2012;13(10):1010–1019.

44. Zhang F, Meng G, Strober W. Interactions among the transcription factors Runx1, RORgammat and Foxp3 regulate the differentiation of interleukin 17-producing T cells. *Nat Immunol*. 2008;9(11):1297–1306.

45. Durant L, et al. Diverse targets of the transcription factor STAT3 contribute to T cell pathogenicity and homeostasis. *Immunity*. 2010;32(5):605–615.

46. Doody KM, Bussières-Marmen S, Li A, Paquet M, Henderson JE, Tremblay ML. T cell protein tyrosine phosphatase deficiency results in spontaneous synovitis and subchondral bone resorption in mice. *Arthritis Rheum*. 2012;64(3):752–761.

47. Yi Z, Lin WW, Stunz LL, Bishop GA. The adaptor TRAF3 restrains the lineage determination of thymic regulatory T cells by modulating signaling via the receptor for IL-2. *Nat Immunol*. 2014;15(9):866–874.

48. Zhou X, et al. Instability of the transcription factor Foxp3 leads to the generation of pathogenic memory T cells in vivo. *Nat Immunol*. 2009;10(9):1000–1007.

49. Bussières-Marmen S, Vinette V, Gungabeesoon J, Aubry I, Pérez-Quintero LA, Tremblay ML. Loss of T-cell protein tyrosine phosphatase in the intestinal epithelium promotes local inflammation by increasing colonic stem cell proliferation. *Cell Mol Immunol*. 2018;15(4):367–376.

50. Rubtsov YP, et al. Regulatory T cell-derived interleukin-10 limits inflammation at environmental interfaces. *Immunity*. 2008;28(4):546–558.

51. Madisen L, et al. A robust and high-throughput Cre reporting and characterization system for the whole mouse brain. *Nat Neurosci*. 2010;13(1):133–140.

52. Lin W, et al. Regulatory T cell development in the absence of functional Foxp3. *Nat Immunol*. 2007;8(4):359–368.

53. Monach PA, Mathis D, Benoist C. The K/BxN arthritis model. *Curr Protoc Immunol*. 2008;Chapter 15:Unit 15.22.